Evolution of dissolved and particulate chromophoric materials during the VAHINE mesocosm experiment in the New Caledonian coral lagoon (South West Pacific)

M. Tedetti[1*], L. Marie[1,2], R. Röttgers[3], M. Rodier[4], F. Van Wambeke[1], S. Helias[1], M. Caffin[1], V. Cornet-Barthaux[1], and C. Dupouy[1]

[1] Aix Marseille Université, CNRS/INSU, Université de Toulon, IRD, Mediterranean Institute of Oceanography (MIO) UM 110, 13288, Marseille, France

[2] Present affiliation: Université de Bretagne Occidentale, IUEM, Lemar UMR CNRS 6539, Place Copernic, F-29280 Plouzané, France

[3] Helmholtz-Zentrum Geesthacht, Centre for Materials and Coastal Research, Institute for Coastal Research, Remote Sensing, Geesthacht, Germany

[4] IRD, Université de la Polynésie française - Institut Malardé - Ifremer, UMR 241, Ecosystèmes Insulaires Océaniens (EIO), IRD Tahiti, PB 529, 98713 Papeete, Tahiti, French Polynesia

[*] Corresponding author: marc.tedetti@mio.osupytheas.fr; Phone: + 33 (0)4 86 09 05 27; Fax: + 33 (0)4 91 82 96 41

For submission to Biogeosciences as a research article for the special issue “Biogeochemical and biological response to a diazotroph bloom in a low-nutrient, low-chlorophyll ecosystem: results from the VAHINE mesocosms experiment”

Revised version 18 May 2016

Abstract

In the framework of the VAHINE project, we investigated the spectral characteristics and the variability of dissolved and particulate chromophoric materials throughout a 23-day mesocosm experiment conducted in the South West Pacific at the exit of the New Caledonian coral lagoon (22°29.073 S - 166°26.905 E) from January 13th to February 4th 2013. Samples were collected in a mesocosm fertilized with phosphate at 1, 6 and 12 m depth and in the surrounding waters. Light absorption coefficients of chromophoric dissolved organic matter (CDOM) [$a_g(\lambda)$] and particulate matter [$a_p(\lambda)$] were determined using a point-source integrating-cavity absorption meter (PSICAM), while fluorescent DOM (FDOM) components were determined from excitation-emission matrices (EEMs) combined with parallel factor analysis (PARAFAC). The evolutions of $a_g(\lambda)$ and $a_p(\lambda)$ in the mesocosm were similar to those of total chlorophyll *a* concentration, *Synechococcus* spp. and picoeukaryote abundances, bacterial production, particulate organic nitrogen and total organic carbon concentrations, with roughly a decrease from the beginning of the experiment to days 9-10, and an increase from days 9-10 to the end of the experiment. In the surrounding waters, the same trend was observed but the increase was much less pronounced, emphasizing the effect of the phosphate fertilization on the mesocosm's plankton community. Correlations suggested that both *Synechococcus* cyanobacteria and heterotrophic bacteria were strongly involved in the production of CDOM and absorption of particulate matter. The increase in phytoplankton biomass during the second part of the experiment led to a higher contribution of particulate material in the absorption budget at 442 nm. The three FDOM components identified (tryptophan-, tyrosine- and UVC humic-like fluorophores) did not follow the evolution of CDOM and particulate matter, suggesting they were driven by different production/degradation processes. Finally, the results of this work support the idea there is

indirect coupling between the dynamics of N_2 fixation and that of chromophoric material *via* the stimulation of *Synechococcus* bloom.

Key words: South West Pacific, mesocosm, CDOM, FDOM, particulate absorption, cyanobacteria.

1. Introduction

Besides water itself, light absorption in the marine environment is due to three main biogeochemical constituents: 1) chromophoric dissolved organic matter (CDOM), also known as gelbstoff, gilvin and yellow substances, and chromophoric particulate matter, subdivided into 2) phytoplankton (photoautotrophic microorganisms), composed of both prokaryotic (cyanobacteria) and eukaryotic species (diatoms, dinoflagellates, coccolithophores,…), and 3) non algal particles (NAP), comprising organic and minerogenic detritus, and heterotrophic organisms. Absorption spectra of CDOM, phytoplankton and NAP have been extensively studied over the last two decades in various oceanic provinces including coastal waters and open ocean (Blough and Del Vecchio, 2002; Babin et al., 2003; Bricaud et al., 2010; Matsuoka et al., 2014). Indeed, in addition to their key role in the oceanic carbon cycle, these three constituents strongly influence the underwater light field and the apparent optical properties of seawater. The knowledge of their absorption spectra is thus essential for bio-optical modeling and remote sensing applications but can be used as well to investigate biological processes in the ocean.

Absorption coefficients of CDOM [$a_g(\lambda)$] and NAP [$a_{nap}(\lambda)$] typically decrease monotonically (exponentially) from ultraviolet (UV, 280-400 nm) to visible (400-700 nm) wavelengths (Nelson et al., 1998; Swan et al., 2009; Tilstone et al., 2012). Even though CDOM absorption spectra are usually featureless, some “shoulders” have been observed sporadically in the UV and visible spectral domains and attributed to the presence of dissolved absorbing pigments released by phytoplankton cells: mycosporine-like amino acids (MAAs) at 310-320 nm or at 330-360 nm, and phaeopigments or non-chlorin metal-free porphyrins at 410-420 nm (Whitehead and Vernet, 2000; Röttgers and Koch, 2012; Organelli et al., 2014; Pavlov et al., 2014). In contrast, absorption coefficients of phytoplankton [$a_\phi(\lambda)$]

100 determined from natural samples commonly display two main peaks in the visible range,
101 around 435-450 and 675 nm, attributable to its content in total chlorophyll *a* (TChl *a* = mono
102 Chl *a* + divinyl Chl *a*) (Lutz et al., 1996; Dupouy et al., 1997; Bricaud et al., 2004), but may
103 also reveal other peaks or shoulders resulting from the presence of other pigments: MAAs at
104 325 nm (Bricaud et al., 2010), TChl *b*, TChl *c* and photoprotective carotenoids at 460-470 nm,
105 photosynthetic carotenoids and photoprotective keto-carotenoids at 490 nm (Carreto, 1985;
106 Stuart et al., 1998; Wozniak et al., 1999; Lohrenz et al., 2003) as well as phycoerythrin at 550
107 nm (Morel, 1997). Hence, while chromophoric detrital matter (CDM = CDOM + NAP) is the
108 major contributor to total absorption in the UV domain (~ 60-95 %), in the blue region (440-
109 490 nm), the contributions of CDM and phytoplankton tend to be equivalent (~ 40-50 %),
110 while CDOM alone is accounting for ~ 80-95 % of CDM in the UV and blue ranges (Siegel et
111 al., 2002; 2005; Tedetti et al., 2010; Nelson and Siegel, 2013).
112 In "Case 1 waters" (Morel and Prieur, 1977), which are generally - but not necessarily -
113 open ocean clear waters, optical properties are controlled by phytoplankton and all its derived
114 material, and TChl *a* concentration may be utilized as an index of optical properties thanks to
115 its covariation with $a_\phi(\lambda)$, $a_g(\lambda)$, $a_{nap}(\lambda)$ and particulate backscattering coefficient [$b_{bp}(\lambda)$]
116 (Antoine et al., 2014). Due to the covariation with $a_\phi(\lambda)$ in Case 1 waters, CDOM is
117 considered as being a by-product of phytoplanktonic production. Nonetheless, recent studies
118 have highlighted some degree of de-phasing between the dynamics in phytoplankton and that
119 of CDOM at the global, regional or seasonal scale (Siegel et al., 2002; Morel et al., 2010;
120 Xing et al., 2014). Whilst photobleaching is now considered as a major degradation process of
121 CDOM in surface waters (Del Vecchio and Blough, 2002; Helms et al., 2008; Bracchini et al.,
122 2010; Swan et al., 2012), the main source of CDOM in open ocean is still a matter of debate,
123 particularly for its "humic-like" component, which absorbs light over a broad range of UV
124 and visible wavelengths and fluoresces in the visible domain (Andrew et al., 2013). Some

works suggest that this humic-like CDOM is in part a remainder of terrestrial matter that has been diluted and transformed during transit to and within the ocean (Blough and Del Vecchio, 2002; Hernes and Benner, 2006; Murphy et al., 2008; Andrew et al., 2013). Conversely, other studies put forward its autochthonous marine source and its production from phytoplankton, including green algal, diatoms, dinoflagellates (Vernet and Whitehead, 1996; Romera-Castillo et al., 2010; 2011; Chari et al., 2013), the diazotrophic (N_2-fixing) cyanobacteria *Trichodesmium* spp. (Subramaniam et al., 1999; Steinberg et al., 2004) and the non-diazotrophic picocyanobacteria *Synechococcus* spp. and *Prochlorococcus* spp. (Romera-Castillo et al., 2011), from zooplankton (Steinberg et al., 2004; Ortega-Retuerta et al., 2009), or from the bacterial degradation (mineralization) of phytoplankton-derived organic matter (Nelson et al., 1998; 2010; Swan et al., 2009).

The New Caledonian coral lagoon, located in the South West Pacific, is a tropical, oligotrophic Low Nutrient Low Chlorophyll (LNLC) ecosystem in which diazotrophs such as cyanobacteria *Trichodesmium* spp. (Dupouy et al., 1988; 2008; Masotti et al., 2007; Rodier and Le Borgne, 2010) and diazotrophic picocyanobacteria (Biegala and Raimbault, 2008) but also non-diazotrophic picocyanobacteria such as *Synechococcus* spp. and *Prochlorococcus* spp. (Biegala and Raimbault, 2008; Neveux et al., 2009) play a significant role. Although the biogeochemical conditions in the New Caledonian coral lagoon are well documented for several years (see review by Grenz et al., 2010), the dynamics of CDOM remains poorly known in this environment. In the framework of the VAriability of vertical and tropHIc transfer of fixed N_2 in the south wEst Pacific (VAHINE) mesocosm experiment, the objectives of the present study were 1) to assess the spectral characteristics and the variability of dissolved and particulate chromophoric materials throughout a 23-day mesocosm experiment, and 2) to tentatively identify the main biogeochemical contributors (diazotrophic and non-diazotrophic primary producers, heterotrophic bacteria) driving changes in

chromophoric material over the course of the experiment. Chromophoric parameters we examined here were absorption coefficients of CDOM [$a_g(\lambda)$] and particulate matter [$a_p(\lambda) = a_\phi(\lambda) + a_{nap}(\lambda)$], determined over the spectral domain 370-720 nm, the spectral slope of CDOM (S_g), computed over the range 370-500 nm, as well as fluorescent DOM (FDOM) components, determined from excitation-emission matrices (EEMs) combined with parallel factor analysis (PARAFAC).

2. Material and methods

2.1. The mesocosm experiment

Study site and mesocosm description. The VAHINE mesocosm experiment was conducted from January 13th to February 4th, 2013 in the South West Pacific at an exit of the New Caledonian coral lagoon, 28 km off the coast of New Caledonia (22°29.073 S - 166°26.905 E) (Fig. 1). At the deployment site the water depth was 25 m and the bottom was sandy. The site was protected by land from the dominant trade winds (SE sector) and characterized by high influence of oceanic oligotrophic waters coming from outside the lagoon through the Boulari passage (Ouillon et al., 2010). Three large mesocosms (hereafter called M1, M2 and M3), of 50 m^3 volume each, were deployed (Fig. 2). All details concerning the mesocosm design and deployment are given in Bonnet et al. (2015). In brief, the mesocosms consisted in large cylindrical bags made of one polyethylene film and one ethylene vinyl acetate (EVA, 19 %) film, each 500 µm thick, with nylon meshing in between to allow maximum resistance and light penetration. They were 2.3 m in diameter, 15 m in depth and were equipped with removable sediment traps allowing collection of sinking material. The top of the bags were maintained 1 m above the surface with floats to prevent inflow of external water. Their straightness was maintained by weights at the bottom of the

mesocosms. Before starting sampling, the mesocosms were left opened from the bottom for 24 h to insure a total homogeneity of the water column.

Nutrient fertilization. To prevent phosphate limitation, the mesocosms were fertilized in the evening of day 4 with dissolved inorganic phosphorus (DIP) to a final concentration of 0.8 µM (see details of the fertilization procedure in Bonnet et al., 2015). This phosphate fertilization aimed at stimulating the diazotroph activity.

Sampling and in situ measurements. During the 23 days of the experiment, seawater sampling was performed every morning from a 4 m^2 floating platform at three depths (1, 6 and 12 m) in each mesocosm and in the surrounding waters close to the mesocosms ("OUT") using a compressed air-driven, metal-free pump (AstiPure™) connected to a polyethylene tubing. Samples were filled into 50-L polypropylene carboys and immediately transported for subsampling and sample treatments onboard the R/V *Alis*, moored 1 nautical mile away from the mesocosm site. Along with discrete sampling, vertical profiles of temperature, salinity, Chl *a* fluorescence, turbidity and light intensity were obtained daily (at 7 a.m. local time) in each mesocosm and in the surrounding waters using a 911plus conductivity temperature depth (CTD) profiler (Sea-Bird Electronics, Inc.). For our specific parameters, i.e. dissolved and particulate chromophoric materials, we only sampled the mesocosm M1 at 1, 6 and 12 m depth and the surrounding waters at 1 m depth.

Filtration. Onboard R/V *Alis*, samples for CDOM absorption and fluorescence measurements were immediately filtered under low vacuum (< 50 mm Hg) through 0.2 µm polycarbonate filters (25 mm diameter, Nuclepore) using small, pre-combusted (450 °C, 6 h) glass filtration systems. Prior to sample filtration, the Nuclepore filters were cleaned by first soaking them for several minutes in 1 M HCl, then in ultrapure water, and processing them by filtering through and discarding 300 mL of ultrapure water and lastly 50 mL of sample. Then, 1 L of sample was filtered and the 0.2 µm filtrate transferred into pre-combusted Schott®

glass bottles for analyses. Powder-free disposable gloves were worn during sampling, filtration and analyses to avoid sample contamination. All absorption coefficient measurements [$a_g(\lambda)$ and $a_{g+p}(\lambda)$] were performed directly onboard (see section 2.2), while samples for fluorescence measurements were stored at 4 °C in the dark for several days until analyses.

The two phases of the experiment. In the results presented below, the 23-day mesocosm experiment was separated into two periods: P1, from day 5 to day 14, and P2, from day 15 to day 23. P1 and P2 denote the two phases of the experiment when the diazotrophic community was dominated by diatom-diazotroph associations (DDAs), more specifically heterocyst-forming *Richelia* associated with *Rhizosolenia*, and unicellular cyanobacteria group C (UCYN-C), respectively (Berthelot et al., 2015; Turk-Kubo et al., 2015).

2.2. Absorption of CDOM and particulate matter

Measurement. Absorption coefficients of CDOM and CDOM + particulate matter [$a_g(\lambda)$ and $a_{g+p}(\lambda)$] were determined by measuring absorption of 0.2 µm filtered and unfiltered samples using a point-source integrating-cavity absorption meter (PSICAM) instrument as described by Röttgers et al. (2007) and Röttgers and Doerffer (2007). The cavity of the PSICAM was filled with purified water (Milli-Q water), air bubbles were removed from the cavity wall and the central light sphere by gentle shaking, and a reference intensity spectrum was recorded between 370 and 726 nm. Afterwards, sample water was poured into the cavity in the same way, and a sample intensity spectrum was recorded. The cavity was rinsed and filled with purified water again, and a second reference intensity spectrum was recorded. The two reference spectra were used to calculate two “transmissions” (sample/reference) and, further, two absorption coefficient spectra. The mean of these two spectra was taken as the real absorption coefficient spectrum. The calibration of the PSICAM consisted of

225 determinations of the total cavity reflectivity spectrum by using solutions of the dye nigrosine
226 (Certistain®, Merck) with maximum absorption between 1 and 3 m^{-1}. Absorption spectra were
227 corrected for salinity and temperature differences between sample and reference water
228 according to Röttgers and Doerffer (2007). The mean precision of the PSICAM within the
229 range 370-700 nm is ± 0.0008 m^{-1}, whereas its accuracy here is ± 2 %, even for absorption
230 values < 0.1 m^{-1}.

231 ***Particulate absorption and CDOM spectral slope determination.*** Absorption
232 coefficients of particulate matter [$a_p(\lambda)$] were determined by subtracting $a_g(\lambda)$ from $a_{g+p}(\lambda)$
233 over the range 370-720 nm. Spectral slope of $a_g(\lambda)$, S_g (in nm^{-1}), was computed by applying a
234 nonlinear (exponential), least-squares fit to the $a_g(\lambda)$ values between 370 and 500 nm in
235 accordance with the following formula:

236 $$a_g(\lambda) = a_g(\lambda 0) \times e^{-S_g(\lambda - \lambda 0)}$$

237 The fit was conducted on raw (i.e. not log-transformed) data according to the
238 recommendations by Twardowski et al. (2004). The average correlation coefficient (r) of the
239 exponential least-squares fits was 1.00 (n = 72). The spectral range used here for the slope
240 determination (370-500 nm) was close to that employed in previous studies for different
241 oceanic waters (i.e. 350-500 nm) (Babin et al., 2003; Röttgers and Doerffer, 2007; Bricaud et
242 al., 2010; Para et al., 2010; Organelli et al., 2014).

243

244 ## 2.3. Fluorescence of DOM

245 ***Measurements.*** FDOM measurements were performed on 0.2-µm filtered samples using
246 a Hitachi F-7000 spectrofluorometer. The correction of spectra for instrumental response was
247 conducted from 200 to 600 nm according to the procedure recommended by the manufacturer
248 (Hitachi F-7000 Instruction Manual) and fully described in Tedetti et al. (2012). The
249 excitation (Ex) and emission (Em) correction curves were applied internally by the instrument

to correct each fluorescence measurement acquired in signal over reference ratio mode. The samples were allowed to reach room temperature in the dark and transferred into a 1-cm pathlength far-UV transparent silica quartz cuvette (170-2600 nm; LEADER LAB). The sample in the cuvette was kept at 20 °C inside the instrument using a circulating water bath connected to the cell holder. The cuvette was cleaned with 1 M HCl and ultrapure water, and triple rinsed with the sample before use. EEMs were generated over λ_{Ex} between 200 and 500 nm in 5-nm intervals, and λ_{Em} between 280 and 550 nm in 2-nm intervals, with 5-nm slit widths on both Ex and Em sides, a scan speed of 1200 nm min^{-1}, a time response of 0.5 s and a PMT voltage of 700 V. Blanks (ultrapure water) and solutions of 0.1 to 10 µg L^{-1} quinine sulphate dihydrate (Fluka, purum for fluorescence) in 0.05 M sulphuric acid were run with each set of samples. Two replicates were run for each sample.

Fluorescence data processing. Different processing steps were carried out on the fluorescence data: 1) all the fluorescence data were normalized to the intensity of the ultrapure water Raman scatter peak at $\lambda_{Ex}/\lambda_{Em}$ of 275/303 nm, measured daily as an internal standard (Coble, 1996). This value varied by 4 % (n = 20). 2) The mean, normalized EEM of ultrapure water was subtracted from normalized sample EEMs to eliminate the water Raman scatter signal. 3) These blank-corrected sample EEMs were converted into quinine sulphate unit (QSU), where 1 QSU corresponded to the fluorescence of 1 µg L^{-1} quinine sulphate at $\lambda_{Ex}/\lambda_{Em}$ of 350/450 nm (5-nm slit widths) (Coble, 1996; Murphy et al., 2008). The conversion in QSU was made by dividing each EEM fluorescence data by the mean slope of a linear regression of fluorescence *vs*. concentration for the different quinine sulphate solutions (i.e. 8.4 arbitrary fluorescence intensity units/QSU). r values of these linear regressions were on average 0.99 and the detection and quantification limits of the fluorescence measurements were 0.19 and 0.63 QSU, respectively. The water Raman scatter peak was integrated from λ_{Em} 380 to 426 nm at λ_{Ex} of 350 nm for ultrapure water samples. The mean value was used to

establish a conversion factor between QSU and Raman unit (RU, nm^{-1}), based on the Raman-area normalized slope of the quinine sulphate linear regression. The conversion factor was 0.025 RU per QSU. Considering the low $a_g(\lambda)$ values, samples were not corrected for inner filter effects (Stedmon and Bro, 2008).

2.4. Parallel factor analysis (PARAFAC)

In this work, a PARAFAC model was created and validated for 130 calibrated EEMs according to the method by Stedmon et al. (2003). The EEM wavelength ranges used were 210-500 and 280-550 nm for Ex and Em, respectively. EEMs were merged into a three-dimensional data array of the form: 130 samples × 59 λ_{Ex} × 136 λ_{Em}. The PARAFAC program was executed using the DOMFluor toolbox v1.6 (Stedmon and Bro, 2008) running under MATLAB® 7.10.0 (R2010a). The full analysis showed that no outliers were present in the dataset. The validation of the PARAFAC model (running with the non-negativity constraint) and the determination of the correct number of components (from 2 to 6 components tested) were achieved through the examination of 1) the percentage of explained variance, 2) the shape of residuals, 3) the split half analysis and 4) the random initialization using the Tucker Congruence Coefficients (Tedetti et al., 2012). The fluorescence intensities of each component found are given in QSU. The fluorescence intensities in QSU provided for each sample is the mean of the two replicates with a coefficient of variance (CV) < 10 %.

2.5. Biogeochemical and biological analyses

Filters for the determination of the TChl *a* concentration were collected by filtering 550 mL of sample water onto a GF/F filter (Whatman). The filters were directly shock-frozen and stored in liquid N_2. TChl *a* was extracted in methanol and measured by fluorometry (Le Bouteiller et al., 1992). The precision of the measurement was ± 0.005 µg L^{-1}.

For the determination of phycoerythrin concentration, water samples (3-4 L) were filtered onto 0.4-µm Nucleopore polycarbonate filters and immediately frozen in liquid N_2 until analysis. Phycoerythrin was extracted in a 4 mL glycerol-phosphate mixture (50/50) according to Neveux et al. (2009) after vigorous shaking for resuspension of particles (Wyman, 1992), and then quantified by fluorometry using a Perkin Elmer LS55 spectrofluorometer (λ_{Ex}: 450-580 nm at λ_{Em} of 605 nm) (Lantoine and Neveux, 1997). The measurement precision was ~ 16 %.

Pico- and nano-phytoplankton abundances were analyzed by flow cytometry. Samples (1.8 mL) were collected from the mesocosm everyday from 1, 6 and 12 m depth in cryotubes, fixed with 200 µL of paraformaldehyde (4 % final concentration), left 15 min at ambient temperature, flash frozen in liquid N_2 and stored at -80 °C until analysis on a FACSCalibur (BD Biosciences) flow cytometer as described in Marie et al. (1999). Before analysis, samples were thawed at ambient temperature in the dark. 600 µL of each sample were mixed and homogenized with 25 µL of TrueCount beads and 10 µL of 2 µm diameter beads (Fluoresbryte^{TM}, Polysciences) used as a reference for size discrimination between pico- and nano-phytoplankton. Phytoplankton communities were clustered as *Prochlorococcus* spp. cell like, *Synechococcus* spp. cell like, nanoeukaryotes cell like and picoeukaryotes cell like according to their optical properties (light scattered and fluorescence emission by the cells) (Marie et al., 1999).

For the determination of microphytoplankton community composition (diatoms), water samples (250 mL) were taken every day by pumping and preserved with formalin. In the laboratory, samples were sedimented and microphytoplankton species were identified and enumerated under inverted microscope.

Bacterial production (BP) was estimated using the ^{3}H-leucine incorporation technique (Kirchman et al., 1985), adapted to the centrifugation method (Smith and Azam, 1992).

Radioactivity was counted using a Liquid Scintillation Analyzer Packard 2100 TR and the ^{3}H counting efficiency was corrected for quenching. BP was calculated from leucine incorporation rates using the conversion factor of 1.5 kg C mol^{-1} leucine, and is shown here in ng C L^{-1} h^{-1}.

Samples for total organic carbon (TOC) concentrations were collected in duplicate in precombusted (4 h, 450 °C), 12-mL sealed glassware flask, acidified with orthophosphoric acid and stored in dark at 4 °C until analysis. Samples were analyzed by using a TOC-5000 total carbon analyzer (Sohrin and Sempéré, 2005). The average TOC concentrations in the Deep Atlantic Water and low carbon water reference standards were 45 ± 2 µM C, n = 24 and 1 ± 0.3 µM C, n = 24, respectively. The analytical precision of the procedure was ≤ 2 %.

Dissolved organic nitrogen (DON) concentrations were calculated from total nitrogen (TN) concentrations subtracted by particulate organic nitrogen (PON) and dissolved inorganic nitrogen (DIN) concentrations. Samples were collected in 50 mL glass bottles and stored at -20 °C until analysis. The samples were divided in two parts after a rapid thaw for analysis of both organic and inorganic concentrations. TN concentration was determined according to the wet oxidation procedure described in Pujo-Pay and Raimbault (1994). Samples for PON concentrations were collected by filtering 1 L of water on GF/F filters and analyzed according to the wet oxidation protocol (Pujo-Pay and Raimbault, 1994) with a precision of 0.06 µM. DIN concentration was determined according to Aminot and Kérouel (2007). Measurements were conducted using a segmented flow auto-analyser (AutoAnalyzer AA3 HR, SEAL Analytical).

2.6. Statistics

Linear regression analyses and one-way analyses of variance (ANOVA) were performed with StatView 5.0 and the statistics package provided in Microsoft Excel 11.0.

ANOVA was used to compare the means of independent data groups (normally distributed). For the different analyses and tests, the significance threshold was set at $p < 0.05$.

3. Results

3.1. Evolution of the core parameters in the mesocosm

The detailed description of temperature, salinity and nutrient concentrations in the three mesocosms is provided in Bonnet et al. (2015). Briefly, water temperature progressively increased inside and outside the mesocosms from 25.4 to 26.2 °C over the course of the 23-day experiment. Salinity also progressively increased from 35.1 to 35.5 but this increase was less pronounced in the surrounding waters with salinities of 35.4 at day 23. Temperature and salinity were homogeneous over depth in the mesocosms, the water column having been well mixed throughout the experiment. In the mesocosms, average concentrations of NO_3^- + NO_2^- were < 0.04 µM before the DIP fertilization (day 4) and decreased to 0.01 µM at the end of the experiment. In contrast, NH_4^+ concentrations were ~ 0.01 µM up to day 18, and then increased up to 0.06 µM at day 23. DIP concentrations increased from 0.02-0.05 µM before the fertilization to 0.8 µM just after, and decreased gradually over time to return to their initial concentrations at day 23 (0.02-0.08 µM). In the surrounding waters, NO_3^- remained < 0.20 µM and DIP was 0.05 µM all over the experiment (Berthelot et al., 2015; Bonnet et al., 2015).

For all the parameters described below, including CDOM and FDOM data, no significant difference was found with depth, except for TChl *a* and PON whose concentrations were higher at 12 m depth than at 1 and 6 m depths (ANOVA, n = 20-22, p = 0.003-0.04). Therefore, in the following paragraphs, the parameter descriptors are generally given in term of depth-averaged values.

3.2. Evolution of phytoplankton biomass, bacterial production and organic N and C pools in the mesocosm

TChl *a*, PON concentrations and BP in the mesocosm M1 and in the surrounding waters (OUT) generally increased throughout the experiment, with a decrease from day 4 to day 9 and then an increase from day 9 to the end of the experiment (Fig. 3a,d,f). This increase was more pronounced in M1, where TChl *a*, PON concentrations and BP varying from 0.12 to 0.55 µg L^{-1}, 0.65 to 1.31 µM and 85 to 681 ng C L^{-1} h^{-1}, respectively. TChl *a*, PON concentrations and BP were significantly higher inside M1 during P2 (day 15 to day 23) than inside M1 during P1 (day 5 to day 14), and than outside during P1 and P2 (ANOVA, n = 25-30, p < 0.0001-0.004) (Table 1). Phycoerythrin concentration decreased from day 4 (0.36 µg L^{-1}) to day 9 (0.05 µg L^{-1}), increased towards day 16 (0.34 µg L^{-1}) and then oscillated to return to the value of 0.34 µg L^{-1} at day 23 (Fig. 3b). In contrast, in OUT, phycoerythrin concentration increased from day 9 to the end of the experiment, showing a strong raise at day 21 (0.85 µg L^{-1}). Thus, during P2, phycoerythrin concentration was significantly higher outside M1 than inside (ANOVA, n = 9, p = 0.004) (Table 1). The TOC concentration decreased from day 4 (70 µM) to day 11 (64 µM) and increased from day 11 to day 22 (81 µM) (Fig. 3c). This increase in the second part of the experiment was not observed in OUT. Although the TOC concentration was significantly higher during P2 than during P1 in M1 (ANOVA, n = 9, p = 0.03), there was no difference between M1 and OUT during P2 (ANOVA, n = 7-9, p = 0.2) (Table 1). The DON concentration was rather constant and only tended to decrease during P2 (Fig. 3e). No significant difference in DON concentrations was found between M1 and OUT (ANOVA, n = 22-29, p = 0.07-0.7) (Table 1).

The abundance of diazotrophs DDAs inside M1 increased from day 3 (77 × 10^3 *nifH* copies L^{-1}) to day 9 (190 × 10^3 *nifH* copies L^{-1}), decreased from day 9 to day 15 (5.4 × 10^3 *nifH* copies L^{-1}) and finally increased from day 15 to day 23 (78 × 10^3 *nifH* copies L^{-1}). In

OUT a quite similar pattern was observed despite a high value of 450×10^3 *nifH* copies L^{-1} at day 18 (Fig. 4a). No significant difference in the abundance of DDAs was observed in M1 between P1 and P2, and between M1 and OUT (ANOVA, n = 3-6, p = 0.05-0.8) (Table 1). On the other hand, the abundance of diazotrophic Group UCYN-C strongly increased from day 9 (0.54×10^3 *nifH* copies L^{-1}) to day 23 (110×10^3 *nifH* copies L^{-1}) in M1, while it increased much more slowly in OUT from day 10 (0.32×10^3 *nifH* copies L^{-1}) to day 22 (4.8×10^3 *nifH* copies L^{-1}) (Fig. 4b). Hence, the abundance of UCYN-C was much higher in M1 during P2 than in M1 during P1 (14 times higher) and than in OUT during P1 and P2 (22-53 times higher) (ANOVA, n = 3-6, $p < 0.0001$) (Table 1). It should be noticed that the abundances of DDAs and UCYN-C are reported as *nifH* (gene) copies L^{-1} rather than cells L^{-1} because there is currently little information about the number of *nifH* copies per genome in these diazotroph targets (Turk-Kubo et al., 2015). Total diatoms in M1 decreased from day 2 (47×10^3 cell L^{-1}) to day 9 (6×10^3 cell L^{-1}) and then oscillated to reach 41×10^3 cell L^{-1} at the end of the experiment, with a maximum value of 120×10^3 cell L^{-1} at day 15 (Fig. 4c). This was essentially due to the large diatom *Cylindrotheca closterium* (data not shown). No difference in abundance of total diatoms was observed between P1 and P2 (ANOVA, n = 5, p = 0.2). The abundances of *Synechococcus* spp., *Prochlorococcus* spp., picoeukaryotes and nanoeukaryotes decreased from day 4 (~ 43, 16, 2.2 and 0.9×10^3 cell mL^{-1}, respectively) to day 9 (~ 18, 5, 0.8 and 0.6×10^3 cell mL^{-1}, respectively) (Fig. 4d-g). From day 9 to the end of the experiment, the abundance of *Synechococcus* spp. and picoeukaryotes noticeably increased to reach ~ 90 and 3.4×10^3 cell mL^{-1} at day 23 respectively, whereas the increase in *Prochlorococcus* spp. and nanoeukaryotes was much less (to ~ 20 and 1.3×10^3 cell mL^{-1} at day 23, respectively). The abundance of *Synechococcus* spp., picoeukaryotes and nanoeukaryotes was significantly higher in P2 than in P1 (ANOVA, n = 23-24, $p < 0.0001$-

0.002), while that of *Prochlorococcus* spp. was not different (ANOVA, n = 23-24, p = 0.07) (Table 1).

3.3. Absorption spectra of CDOM and particulate matter

CDOM absorption spectra of samples collected in M1 and OUT were quite similar, displaying an exponential decrease in $a_g(\lambda)$ without any significant shoulder (Fig. 5). $a_p(\lambda)$ spectra, which reflect the absorption by both phytoplankton and NAP, were characterized by two main Chl *a* peaks, one between 432 and 442 nm (at 436 nm on average) and one between 672 and 682 nm (at 676 nm on average), while several shoulders also emerged at 376, 416, 464, 490 and 550 nm (Fig. 5). Hereafter, $a_g(\lambda)$ is presented at 370 and 442 nm, while $a_p(\lambda)$ is given at 442 and 676 nm, the two latter wavelengths corresponding to the absorption maxima of Chl *a*.

3.4. Evolution of absorption coefficients, spectral slope in the mesocosm

In M1, absorption coefficients decreased from day 4 to day 9 and then increased from day 9 to the end of the experiment (day 23), leading to variations in the ranges 0.041-0.067 m^{-1} for $a_g(370)$, 0.011-0.020 m^{-1} for $a_g(442)$, 0.009-0.025 m^{-1} for $a_p(442)$ and 0.003-0.012 m^{-1} for $a_p(676)$ (Fig. 6a,b,d,e). In OUT, these parameters also increased from day 9 or 10 to day 23 but with lower amplitude. Inside M1, all these absorption coefficients were significantly higher during P2 than during P1 (ANOVA, n = 27-30, $p < 0.0001$). However, only $a_g(370)$ and $a_p(442)$ were significantly higher in M1 than outside during P2 (ANOVA, n = 9-27, p = 0.004-0.02) (Table 1). S_g inside and outside M1, ranging from 0.0148 to 0.0188 nm^{-1}, did not display any clear pattern throughout the experiment (Fig. 6c).

3.5. Spectral characteristics and identification of FDOM components

Three FDOM components (C1-C3) were identified by the PARAFAC model validated on 130 EEM samples from M1 and OUT. The spectral characteristics of C1-C3 are reported in Fig. 7. These components exhibited one or two Ex maxima and one Em maximum. C1, with a maximum at $\lambda_{Ex}/\lambda_{Em}$ of 230/476 nm, corresponded to the category of UVC humic-like fluorophores, referred to as peak A (Coble, 1996; 2007; Ishii and Boyer, 2012). C2 and C3 had two maxima each, located at λ_{Ex1}, $\lambda_{Ex2}/\lambda_{Em}$ of 225, 280/344 nm and 225, 275/304 nm, respectively (Fig. 7). They belonged to the group of protein-like fluorophores, C2 being analogous to tryptophan-like fluorophore (peaks T) and C3 being analogous to tyrosine-like fluorophore (peaks B) (Coble, 1996; 2007).

3.6. Evolution of FDOM components in the mesocosm M1

Inside M1, the fluorescence intensity of humic-like fluorophore decreased from day 2 (~ 5.3 QSU) to day 8 (~ 2.7 QSU), increased from day 8 to day 14 (~ 4.8 QSU) and dropped down to ~ 2.5 QSU at day 15. Then, it increased to reach ~ 5.6 QSU at day 20 (Fig. 8a). The fluorescence intensity of tryptophan-like fluorophore decreased from day 3 (~ 9.1 QSU) to day 8 (~ 5.3 QSU) (Fig. 8b). At day 9, it increased up to ~ 8.3 QSU and remained relatively stable up to day 14 (~ 8.4 QSU). After a reduction at day 15 (~ 5.9 QSU), the fluorescence intensity increased up to the end of the experiment (~ 10.4 QSU at day 20). The fluorescence intensity of tyrosine-like fluorophore decreased from day 5 (~ 8.2 QSU) to day 15 (~ 3.9 QSU) and then slowly increased to day 20 (~ 6.2 QSU) (Fig. 8c). While for humic- and tryptophan-like fluorophores no differences in their fluorescence intensity were observed between P1 and P2 (ANOVA, n = 18-30, p = 0.4-0.9), the fluorescence intensity of tyrosine-like fluorophore was significantly lower during P2 (ANOVA, n = 18-28, p = 0.002) (Table 1). Overall, the FDOM pool was dominated by protein-like material: the combined fluorescence

of tryptophan and tyrosine fluorophores ranged from 9.1 to 22.3 QSU, while the fluorescence of humic fluorophore ranged from 1.9 to 6.2 QSU.

3.7. Relationships between the chromophoric and the biogeochemical/biological parameters

Table 2 presents *r* values of linear regressions between the chromophoric and the biogeochemical/biological parameters for the samples collected in M1 from day 5 to day 20. Here we consider that only the correlations that are very highly significant ($p < 0.0001$) reflect relevant linear relationships. $a_g(370, 442)$ and $a_p(442, 676)$ were not that much correlated to each other ($r = 0.52$-0.62, $n = 36$, $p < 0.0001$-0.002). S_g was not correlated to $a_g(370, 442)$ ($r = 0.15$-0.22, $n = 36$, $p = 0.06$-0.9). Even though humic- and tryptophan-like fluorophores were very highly correlated ($r = 0.67$, $n = 36$, $p < 0.0001$), they did not show any coupling with tyrosine-like fluorophore ($r = 0.20$-0.48, $n = 36$, $p = 0.005$-0.2). Moreover, none of these three fluorophores was very highly correlated to the absorption coefficients and spectral slope ($r = 0.09$-0.42, $n = 36$, $p > 0.5$-0.05) (Table 2). These correlations emphasize the decoupling between the CDOM and FDOM materials during the experiment.

All absorption coefficients were very highly positively correlated to *Synechococcus* spp. abundance ($r = 0.76$-0.83), BP ($r = 0.72$-0.78), TChl *a* concentration ($r = 0.60$-0.88), PON concentration ($r = 0.58$-0.75) and picoeukaryote abundance ($r = 0.52$-0.71) ($n = 36$, $p < 0.0001$). Linear relationships between $a_g(370)$ or $a_p(442)$ and *Synechococcus* spp. abundance are presented in Fig. 9. S_g as well as the three FDOM fluorophores did not present any highly significant correlation with the biogeochemical/biological constituents. Phycoerythrin, TOC, DDAs, UCYN-C and total diatoms did not display any very highly significant correlations with the chromophoric parameters although some *r* values were quite high [for instance 0.90 between UCYN-C and $a_p(442)$]. This is because these correlations were determined for a

lower number of samples (8-15). Nonetheless, albeit not very highly significant, these relationships highlighted interesting trends such as positive (negative) relationships between absorption coefficients (tyrosine-like fluorophore) and UCYN-C abundance, and negative (positive) relationships between absorption coefficients (tyrosine-like fluorophore) and DDA abundance (Table 2).

4. Discussion

4.1. General characteristics of chromophoric material

CDOM absorption. CDOM absorption spectra from samples inside and outside the mesocosm did not display any significant shoulder in the range 370-720 nm (Fig. 5). In the same way, using the PSICAM, Röttgers and Koch (2012) did not observe any specific feature in the CDOM absorption spectra from 380 to 700 nm of samples collected in the surface waters of the tropical Atlantic Ocean and of the North East and South West Pacific, including our study area inside the barrier reef of New Caledonia.

$a_g(370)$ and $a_g(442)$ measured inside and outside the mesocosm (0.040-0.086 and 0.011-0.022 m^{-1}, respectively; Fig. 6a,b) were within the range of those measured in surface waters of the Atlantic Ocean and at 80-200 m depth in the South West Pacific (offshore of New Caledonia) (0.021-0.118 and 0.004-0.039 m^{-1}, respectively) (Röttgers and Doerffer, 2007; Röttgers and Koch, 2012; Dupouy et al., 2014). In addition, our $a_g(370)$ and $a_g(442)$ values were slightly lower than those measured in the subtropical North Pacific and the Mediterranean Sea (0.050-0.090 and 0.018-0.035 m^{-1}, respectively) (Yamashita et al., 2013; Organelli et al., 2014) but higher than those observed in the center of the gyre of the South East Pacific (> 0.010-0.035 and 0.005-0.015 m^{-1}, respectively) (Bricaud et al., 2010).

Our S_g values determined over the range 370-500 nm varied between 0.015 and 0.019 nm^{-1} inside and outside the mesocosm (Fig. 6c). They were to some extent lower than S_g values determined between 350 and 500 nm of surface waters of the Mediterranean Sea, Atlantic Ocean and South East Pacific (0.015-0.025 nm^{-1}) (Röttgers and Doerffer, 2007; Bricaud et al., 2010; Para et al., 2010; Organelli et al., 2014). In fact, our S_g values did not reach the maximal values encountered in oligotrophic areas (0.020-0.025 nm^{-1}) despite the potentially important CDOM photobleaching processes which would have occurred in the surface waters of the mesocosm. This is explained by the different spectral ranges used for the S_g determination (370-500 nm *vs* 350-500 nm). Indeed, S_g, which strongly depends on the chosen wavelength interval, is generally higher for intervals in the short wavelengths (Nelson and Siegel, 2013; Sempéré et al., 2015), and do not present a constant spectral slope but rather steeper slopes towards the short UV wavelengths (Tedetti et al., 2007; Sempéré et al., 2015). Hence, this difference of 20 nm in the wavelength interval may influence the S_g values, the latter decreasing when considering the range 370-500 nm. It is worth noting that no correlation was found between $a_g(370)$ or $a_g(442)$ and S_g (Table 2). This was probably attributable to the low ranges and the low values of both $a_g(\lambda)$ and S_g reported here.

FDOM. The three FDOM components identified in this work were UVC humic-, tryptophan- and tyrosine-like fluorophores (Fig. 7). Thus, FDOM was dominated by protein-like material, i.e. compounds containing nitrogen, while humic-like material was less represented. Of these protein-like compounds, tryptophan- and tyrosine-like fluorophores have been reported in many aquatic ecosystems (see reviews by Coble, 2007; Fellman et al., 2010). They represent compounds of low molecular weight at the state of free amino acids or amino acids bound in peptides or proteins. They are known to be released by autochthonous (marine) phytoplankton activity and serve as fresh and labile bioavailable products for heterotrophic bacteria (Yamashita and Tanoue, 2004; Nieto-Cid et al., 2006; Davis and

547 Benner, 2007; Romera-Castillo et al., 2010; Tedetti et al., 2012). Moreover, they can be
548 directly associated to humic substances (Stedmon and Cory, 2014). Generally, they do not
549 show any conservative behaviour in the salinity gradient (Kowalczuk et al., 2009). UVC
550 humic-like fluorophore ("peak A") corresponds to component 1 ($\lambda_{Ex}/\lambda_{Em}$: < 230-260/400-500
551 nm) in the review paper by Ishii and Boyer (2012) and is one of the most widespread humic-
552 like components in the aquatic environment (Kowalczuk et al., 2009; 2013). This fluorophore,
553 which absorbs light at very short wavelengths (230 nm) and fluoresce in long visible
554 wavelengths (476 nm) resulting in a high Stokes shift (246 nm), would be of relatively low
555 molecular weight (< 1 kDa) compared to other fluorescent humic-like materials (Ishii and
556 Boyer, 2012). Present in higher quantities in the photic zone and shallow surface waters, this
557 humic-like component is recognized as a photodegradation product of marine organic matter
558 (Yamashita et al., 2008; Ishii and Boyer, 2012) and appears to be resistant to biodegradation
559 (Balcarczyk et al., 2009; Fellman et al., 2010; Lønborg et al., 2015).
560 ***Particulate absorption.*** Particulate absorption coefficient spectra were dominated by
561 phytoplankton absorption [$a_\phi(\lambda)$] with the presence of the two main peaks of Chl *a* (at 436 and
562 672 nm), whereas the influence of detrital material (NAP), characterized by an exponential
563 decrease of absorption with wavelength, was not really visible upon these spectra (Fig. 5).
564 Besides these two main peaks, several shoulders were found between 376 and 550 nm.
565 Actually, the shoulders at 376 and 416 nm might be related to Chl *a* (Stuart et al., 1998;
566 Lohrenz et al., 2003). The shoulders at 464 and 490 nm reflected the occurrence of
567 photosynthetic carotenoids and/or non photosynthetic (photoprotective) carotenoids (Dupouy
568 et al., 1997; 2003; Stuart et al., 1998; Wozniak et al., 1999; Lohrenz et al., 2003; Bricaud et
569 al., 2004). In addition, the shoulder at 490 nm may be related to the presence of phycourobilin
570 (PUB). PUB, which absorbs light around 490 nm, is known to be contained in phycoerythrin
571 of cyanobacteria, such as *Synechococcus* spp., living in the open ocean. PUB is indeed

572 considered as a chromatic adaptation to blue radiation which penetrates deeper than other
573 wavelengths in the water column (Neveux et al., 1999). Also, the small shoulder at 550 nm
574 could be the sign of phycoerythrobilin (PEB), also contained in phycoerythrin. PEB,
575 absorbing light around 550-565 nm, is present in higher amount in *Synechococcus* spp. of
576 coastal environments (Neveux et al., 1999). Pronounced shoulders or peaks at 550 nm are
577 observed only for exceptional *Synechococcus* spp. concentrations ($> 3 \times 10^5$ cell mL^{-1}) with
578 TChl *a* > 1 µg L^{-1} (Morel, 1997) or more commonly for large filamentous cyanobacteria in
579 tropical waters (Dupouy et al., 2008). An attribution of the shoulders at 490 and 550 nm to
580 PUB and PEB, respectively appears reasonable regarding the fact that PUB and PEB signals
581 were detected in the phycoerythrin fluorescence measurements (M. Rodier, pers. comm.).
582 Such a proportion of *Prochlorococcus* spp. and *Synechococcus* spp. counts reported in this
583 work are typical of the New Caledonia lagoon (Neveux et al., 2009) compared to the
584 equatorial upwelling area where this is inversed (Dupouy et al., 2003).
585 Absorption coefficients of particulate matter at 442 and 676 nm [$a_p(442)$ and $a_p(676)$]
586 measured inside and outside the mesocosm at the exit of the New Caledonian coral lagoon
587 (0.006-0.031 and 0.0013-0.013 m^{-1}, respectively; Fig. 6d,e) were slightly lower than those
588 measured with the same instrument in the surface waters within the New Caledonian lagoon
589 (0.008-0.040 and 0.0030-0.018 m^{-1}, respectively) (Röttgers et al., 2014; Dupouy et al., 2014),
590 the latter values being linked to an exceptional increase in total phytoplankton biomass during
591 the 2008 Valhybio cruise in response to a *La Nina* heavy rain episode (Dupouy et al., 2009;
592 Fuchs et al., 2012).
593
594 **4.2. Coupling between the dynamics of chromophoric material and that of**
595 **N_2 fixation in the mesocosm**

Link between absorption and Synechococcus spp. Several observations suggest the observed change in particulate matter absorption [$a_p(\lambda)$] during the experiment was mainly driven by *Synechococcus* spp. Several observations may support this hypothesis. Firstly, *Synechococcus* spp. was the most abundant group among (non-diazotrophic) pico-, nano- and micro-phytoplankton communities in the mesocosm (Fig. 4c-g). For instance, the concentration of *Synechococcus* spp. ($88 \pm 14 \times 10^3$ cell mL^{-1} in P2) was higher by a factor ~ 1000 relative to that of total diatoms ($44 \pm 37 \times 10^3$ cell L^{-1} in P2) (Table 1). *Synechococcus* spp. abundance cannot in first approach be compared to those of diazotrophs (given in *nifH* copies L^{-1}). However, assuming that there was a minimum of one *nifH* gene copy per cell, the number of *nifH* (gene) copies L^{-1} may reflect the upper limit of the number of cells L^{-1}, though DNA and RNA extractions were probably < 100% (Foster et al., 2009). In this sense, the concentration of *Synechococcus* spp. was higher by a factor ~ 1000 relative to that of UCYN-C ($64 \pm 24 \times 10^3$ *nifH* copies L^{-1}, given a maximum of $64 \pm 24 \times 10^3$ cell L^{-1} in P2) (Table 1). Thus, we conclude that *Synechococcus* spp. was very likely the most important group among non-diazotrophic and diazotrophic communities in the mesocosm. Secondly, *Synechococcus* spp. is known to have significant absorption properties in the visible domain, highlighted in culture experiments (Bidigare et al., 1989; Morel et al., 1993; Stramski and Mobley, 1997; Lutz et al., 2001) but also in natural samples (Morel, 1997). Absorption properties of *Synechococcus* spp. have been compared to those of *Prochlorococcus* spp. and nanoplanktonic diatoms. The efficiency factor for absorption (given for a cell), which depends on both the size and the internal pigment concentration, was on average two times higher for *Prochlorococcus* spp. and three times higher for nanoplanktonic diatoms than for *Synechococcus* spp. over the visible domain (Morel et al., 1993; Stramski and Mobley, 1997). Considering than the number of cells of *Synechococcus* spp. was on average 6 times higher than that of *Prochlorococcus* spp. and ~ 1000 times higher than that of total diatoms during

P2, we may put forward that *Synechococcus* spp was the main contributor to visible absorption in the mesocosm. Finally, $a_p(442)$ and $a_p(676)$ showed the highest positive correlation with *Synechococcus* spp. abundance (Table 2; Fig. 9) with a very similar evolution during P1 and P2 (Fig. 4d, 6d,e).

The absorption of CDOM also presented the highest (positive) coupling with *Synechococcus* spp. abundance and BP (Fig. 3f, 4d, 6a,b; Table 2; Fig. 9), thereby suggesting CDOM was produced by heterotrophic bacteria from their assimilation of labile organic compounds released by *Synechococcus* spp. Indeed, the latter has been shown to release DOM (Bronk, 1999; Becker et al., 2014) that may be directly used to support heterotrophic activity (Nagata, 2000; Lefort and Gasol, 2014). These (non-colored) labile organic substrates issued from *Synechococcus* spp. would be converted into chromophoric, more refractory compounds by heterotrophic bacteria (Nelson et al., 1998; Rochelle-Newall and Fisher, 2002; Nelson and Siegel, 2013). Currently, the coupling between phytoplankton and heterotrophic bacteria seems to be recognized as a major pathway for the formation of CDOM in the ocean (Rochelle-Newall and Fisher, 2002; Nelson and Siegel, 2013; Organelli et al., 2014). Interestingly, Biers et al. (2007) highlighted the role of DON, specifically amino sugars and aromatic amino acids, in the microbial production of CDOM and FDOM while Bronk et al. (1999) reported the production of DON by *Synechococcus* spp. Consequently, the works by Biers et al. (2007) and Bronk et al. (1999) support the assumption of the CDOM production by heterotrophic bacteria consecutive to their utilization of labile DOM (that would be in part in the form of DON) released by *Synechococcus* spp. cyanobacteria. CDOM could be also produced directly from *Synechococcus* spp., as mentioned by Romera-Castillo et al. (2011). Also, we cannot exclude the participation of other primary producers, such as diatoms, to the CDOM production through a direct release of colored material (Romera-Castillo et al., 2010; Chari et al., 2013) or through the bacterial re-working. For example, from culture

experiments, Chari et al. (2013) reported the production of CDOM by *Cylindrotheca closterium*, one of the most important diatom species in the mesocosm. Regarding the respective abundances of *Synechococcus* spp. and diatoms and their evolution all over the experiment, it seems however that *Synechococcus* spp. was a greater contributor to CDOM than diatoms. Consequently, even though it seems difficult here to discriminate the respective contributions of cyanobacterial primary producers (*Synechococcus* spp.) and heterotrophic bacteria in the production of CDOM, unambiguously the coupling between both plays a key role in the absorption of particulate and dissolved chromophoric material in the mesocosm.

Link between absorption, Synechococcus spp. and N_2 fixation. During the first part of the experiment (P1), the diazotrophic community was dominated by diatoms-diazotrophs associations (DDAs) (Fig. 4a), more specifically heterocyst-forming *Richelia* associated with *Rhizosolenia* (Turk-Kubo et al., 2015). The decrease observed in phytoplankton biomass (including diatoms, *Synechococcus* spp., *Prochlorococcus* spp., pico- and nano-eukaryotes), BP and organic C/N pools from day 4 to day 9-11 (Fig. 3a-d,f; Fig. 4c-g) was attributable to a N limitation. In fact, during the first days, phytoplankton would have consumed the small stock of nitrates remaining in the water column without new inputs. In addition, DDAs would not have been a significant source of N for its surrounding environment because *Richelia* would have given the major part of the N that they had fixed to their host diatoms (Berthelot et al., 2015). This decrease in *Synechococcus* spp. and BP led to the decrease in CDOM and particulate matter absorption (Fig. 6a,b,d,e). During P1, the total amount of N issued from the N_2 fixation was equivalent to the total amount of PON exported, suggesting there is a rapid and possibly direct export of the recently fixed N_2 by DDAs (Berthelot et al., 2015). In the second part of the experiment (P2), unicellular cyanobacteria Group C (UCYN-C) became the dominant diazotrophs (Fig. 4b). The UCYN-C bloom was induced by the phosphate fertilization and increasing temperatures (Turk-Kubo et al., 2015). Consequently, N_2 fixation

671 rates were higher during P2 than during P1 (Berthelot et al., 2015). From these authors, the N
672 released by UCYN-C (in the form of DON and/or NH_4^+) allowed for supporting non-
673 diazotrophic cyanobacterial and heterotrophic bacterial growths. This would have in turn
674 stimulated the production of dissolved and particulate chromophoric materials [increase in
675 TChl *a*, PON, TOC, BP, *Synechococcus* spp., $a_g(370, 442)$ and $a_p(442, 676)$ from day 9-11 to
676 day 21-23; Fig. 3a,c,d,f; Fig. 4d; Fig. 6a,b,d,e]. The enhancement of *Synechococcus* spp. *via*
677 the release of N by diazotrophs has been already underscored by Agawin et al. (2007). This N
678 release could also explain the strong increase in diatoms (mainly *Cylindrotheca closterium*) at
679 day 15 (Fig. 4c). In P2, both N_2 fixation and DON consumption were significant N sources
680 for primary production and might explain the PON production (Berthelot et al., 2015). It is
681 worth noting that a perfect temporal synchronization occurred between the variations of
682 *Synechococcus* spp./BP and the variations of CDOM and particulate matter absorption. This
683 implies rapidity in the production mechanisms of the chromophoric material inside the
684 mesocosm. The variations of S_g (Fig. 6c) [no correlation with $a_g(370, 442)$; Table 2]
685 suggested that CDOM absorption was not only influenced by production processes but was
686 also probably affected by photo- and microbial-degradation processes. It is very likely that
687 these degradation processes were not intense enough to counterbalance the production of
688 CDOM by the couple *Synechococcus* spp./heterotrophic bacteria.

689 ***Absorption budget.*** Also, the contribution of CDOM (a_g) to the total absorption (a_{g+p})
690 remained high in the UV domain (370 nm), ranging from 72 to 96 %, while it decreased from
691 the beginning (50-66 %) to the end of the experiment (40-48 %) in the visible domain (442
692 nm). These percentages in the UV and visible domains are in line with those reported in the
693 literature for the open ocean (Siegel et al., 2002; 2005; Tedetti et al., 2010), the higher
694 contribution of particulate material in the absorption budget at 442 nm during the second part

of the experiment being explained by the bloom of cyanobacterial primary producers (*Synechococcus* spp.).

FDOM decoupling. FDOM did neither follow the evolution of CDOM nor the evolution of heterotrophic bacteria and *Synechococcus* spp. (Fig. 8; Table 2). The evolution of tyrosine-like fluorophore, whose fluorescence intensity was higher in P1 than in P2 (Table 1), tended to be close to that of DDAs (Fig. 4a, 8c; Table 2). Therefore, we may hypothesize a role of these diatoms-diazotrophs associations in the production of the tyrosine-like material. The tyrosine-like fluorophore released by phytoplankton could then be consumed by heterotrophic bacteria as labile substrates. UVC humic-like fluorophore displayed an evolution close to that of tryptophan material with two important decreases at days 7-8 and 15. This observation supports the hypothesis by Stedmon and Cory (2014) of an association between humic substances and tryptophan fluorophore in seawater. This revealed that the humic-like component was also subjected to production/degradation processes in the mesocosm that cannot be precisely identified here. The fact that CDOM which absorbs light at 370 nm was not fluorescent (no fluorophores with Ex peak at 370 nm) strengthened the assumption that $a_g(370)$ and the three fluorophores represented independent chromophoric materials that were driven by different processes. Also, these fluorophores could be not major components of the CDOM. Consequently, they would absorb but not strongly enough to significantly affect the CDOM variability. Tryptophan- and tyrosine-like fluorophores belonged to the DON pool. Nonetheless, they showed different patterns in the mesocosm: while DON decreased during P2 (both the DON consumption and the N_2 fixation supported the PON production during P2; Berthelot et al., 2015), the two fluorophores tended to increase. This suggested that tryptophan- and tyrosine-like materials were probably not involved in the PON production.

5. Conclusion

Studies dealing with the CDOM dynamics in the frame of mesocosm experiments remain limited so far and have been conducted merely in coastal-temperate or polar ecosystems (Rochelle-Newall et al., 1999; 2004; Pavlov et al., 2014). This work highlights the spectral characteristics and the variability of dissolved and particulate chromophoric materials throughout a 23-day mesocosm experiment in a tropical, oligotrophic LNLC ecosystem in which N_2 fixers and picophytoplankton play an essential role. Although CDOM did not display any specific shoulders in its absorption spectra, those of particulate chromophoric material were dominated by Chl *a* fingerprint with small signatures of carotenoids, phycourobilin and phycoerythrobilin, which could be related to *Synechococcus* spp., the most abundant cyanobacterial group in the mesocosm. The dynamics of CDOM and particulate matter were strongly coupled with those of *Synechococcus* spp. and bacterial production. Indeed, in the second part of the experiment, the N released in the surrounding environment, very likely by UCYN-C diazotrophs, allowed for supporting cyanobacterial and heterotrophic bacterial growths and subsequently stimulating the production of dissolved and particulate chromophoric materials. The increase in phytoplankton biomass during the second part of the experiment led to a higher contribution of particulate material in the absorption budget at 442 nm. FDOM, composed by (N-containing) protein-like fluorophores and UVC humic-like (photoproduct) fluorophore, did not follow the evolution of CDOM and particulate matter, and was thus subjected to different production/degradation processes in the mesocosm. Finally, this study strongly supports the idea of an indirect link between the dynamics of the N_2 fixation and that of chromophoric material in the South West Pacific.

Acknowledgements. Funding for this research was provided by the Agence Nationale de la Recherche (ANR starting grant VAHINE ANR-13-JS06-0002), INSU-LEFE-CYBER program, GOPS, IRD and M.I.O. The authors thank the captain and crew of the R/V *Alis*. We acknowledge the SEOH divers service from the IRD research center of Noumea (E. Folcher, B. Bourgeois and A. Renaud) and from the Observatoire Océanologique de Villefranche-sur-mer (OOV, J.M. Grisoni) as well as the technical service of the IRD research center of Noumea for their helpful technical support. C. Guieu, F. Louis and J.M. Grisoni from OOV are warmly thanked for the mesocosms design and their useful advice for deployment. We also thank A. Desnues, B. Charrière, H. Berthelot, J. Héliou and T. Moutin for their help and assistance in the sampling and analyses. S. Bonnet, PI of the VAHINE project, and J. Neveux are greatly acknowledged for their constructive comments and discussions on the early versions of the manuscript. Two anonymous Reviewers are acknowledged for their relevant comments and corrections, which contributed to improve the quality of this manuscript.

References

Agawin, N. S. R., Rabouille, S., Veldhuis, M. J. W., Servatius, L., Hol, S., van Overzee, H. M. J., et al. : Competition and facilitation between unicellular nitrogen-fixing cyanobacteria and non-nitrogen-fixing phytoplankton species, Limnol. Oceanogr. 52, 2233–2248, 2007.

Aminot, A., and Kérouel, R.: Dosage automatique des nutriments dans les eaux marines : méthodes en flux continu. Ed. Ifremer, Méthodes d'analyse en milieu marin 188 p., 2007.

Andrew, A. A., Del Vecchio, R., Subramaniam, A., and Blough, N. V.: Chromophoric dissolved organic matter (CDOM) in the Equatorial Atlantic Ocean: Optical properties and their relation to CDOM structure and source, Mar. Chem., 148, 33–43, 2013.

Antoine, D., Babin, M., Berthon, J. F., Bricaud, A., Gentili, B., Loisel, H., Maritorena, S., and Stramski, D.: Shedding Light on the Sea: André Morel's Legacy to Optical Oceanography, Ann. Rev. Mar. Sci., 6, 15.1–15.21, 2014.

Babin, M., Stramski, D., Ferrari, G. M., Claustre, H., Bricaud, A., Obolensky, G., and Hoepffner, N.: Variations in the light absorption coefficients of phytoplankton, nonalgal particles, and dissolved organic matter in coastal waters around Europe, J. Geophys. Res., 108(C7), 3211, doi:10.1029/2001JC000882, 2003.

Balcarczyk, K. L., Jones, J. B. Jr, Jaffe, R., and Maie, N.: Stream dissolved organic matter bioavailability and composition in watersheds underlain with discontinuous permafrost, Biogeochemistry, 94, 255−270, 2009.

Becker, J. W., Berube, P. M. Follett, C. L., Waterbury, J. B., Chisholm, S. W., Delong, E. F., and Repeta, D. J., 2014. Closely related phytoplankton species produce similar suites of dissolved organic matter, Front. Microbiol., 5, 111, 2014.

Berthelot, H., Moutin, T., L'Helguen, S., Leblanc, K., Hélias, S., Grosso, O., Leblond, N., Charrière B., and Bonnet S.: Dinitrogen fixation and dissolved organic nitrogen fueled

primary production and particulate export during the VAHINE mesocosms experiment (New Caledonia lagoon), Biogeosciences, 12, 4273–4313, 2015.

Bidigare, R., Schofield, O., and Prezelin, B.: Influence of zeaxanthin on quantum yield of photosynthesis of Synechococcus clone WH 7803 (CD2), Mar. Ecol. Prog. Ser., 56, 177–188, 1989.

Biegala, I. C., and Raimbault, P.: High abundance of diazotrophic picocyanobacteria (< 3 µm) in a Southwest Pacific coral lagoon, Aquat. Microb. Ecol., 51, 45–53, 2008.

Biers, E. J., Zepp, R. G., Moran, M. A.: The role of nitrogen in chromophoric and fluorescent dissolved organic matter formation, Mar. Chem., 103, 46–60, 2007.

Blough, N. V., and Del Vecchio, R.: Chromophoric DOM in the coastal environment. In: Hansel, D.A., Carlson, C.A. (Eds.), Biogeochemistry of Marine Dissolved Organic Matter. Academic Press, San Diego, California, pp. 509–546, 2002.

Bonnet, S., Moutin, T., Rodier, M., Grisoni, J. M., Louis, F., Folcher, E., Bourgeois, B., Boré, J. M., and Renaud, A.: Introduction to the project VAHINE: VAriability of vertical and tropHIc transfer of diazotroph derived N in the south wEst Pacific, Biogeosciences Discuss., doi:10.5194/bg-2015-615, in review, 2016.

Bracchini, L., Tognazzi, A.,Dattilo, A. M., Decembrini, F., Rossi, C., and Loiselle, S. A.: Sensitivity analysis of CDOM spectral slope in artificial and natural samples: an application in the central eastern Mediterranean Basin, Aquat. Sci., 72, 485–498, 2010.

Bricaud, A., Babin, M., Claustre, H., Ras, J., and Tièche, F.: Light absorption properties and absorption budget of Southeast Pacific waters, J. Geophys. Res., 115, C08009, doi:10.1029/2009JC005517, 2010.

Bricaud, A., Claustre, H., Ras, J., and Oubelkheir, K.: Natural variability of phytoplanktonic absorption in oceanic waters: Influence of the size structure of algal populations, J. Geophys. Res., 109, C11010, doi:10.1029/2004JC002419, 2004.

809 Bronk, D. A.: Rates of NH_4^+ uptake, intracellular transformation, and dissolved organic
810 nitrogen release in two clones of marine *Synechococcus* spp, J. Plankton Res., 21, 1337–
811 1353, 1999.
812 Carreto, J.J.: A new keto-carotenoid from the dino-flagellate *Protopendinium depressurn*
813 (Bayley) Balech, 1974, J. Plankton Res., 7, 421–423, 1985.
814 Carreto, J.I., and Carignan, M. O.: Mycosporine-like amino acids: relevant secondary
815 metabolites. Chemical and ecological aspects, Mar. Drugs, 9, 387–446, 2011.
816 Chari, N. V. H. K., Keerthi, S., Sarma, N. S., Rao Pandi, S., Chiranjeevulu, G., Kiran, R., and
817 Koduru, U.: Fluorescence and absorption characteristics of dissolved organic matter
818 excreted by phytoplankton species of western Bay of Bengal under axenic laboratory
819 condition, J. Exper. Mar. Biol. Ecol., 445, 148–155, 2013.
820 Coble, P. G.: Characterization of marine and terrestrial DOM in seawater using excitation
821 emission matrix spectroscopy, Mar. Chem., 51, 325–346, 1996.
822 Coble, P. G.: Marine optical biogeochemistry – the chemistry of ocean color, Chem. Rev.,
823 107, 402–418, 2007.
824 Davis, J., and Benner, R: Quantitative estimates of labile and semi-labile dissolved organic
825 carbon in the western Arctic Ocean: A molecular approach, Limnol. Oceanogr., 52, 2434–
826 2444, 2007.
827 Del Vecchio, R., and Blough, N. V.: Photobleaching of chromophoric dissolved organic
828 matter in natural waters: Kinetics and modelling, Mar. Chem. 78, 231–253, 2002.
829 Dupouy, C., Frouin, R., Röttgers, R., Neveux, J., Gallois, F., Panché, J. Y., Gérard, P.,
830 Fontana, C., Pinazo, C., Ouillon, S., and Minghelli-Roman, A.: Ocean color response to an
831 episode of heavy rainfall in the lagoon of New Caledonia, Proc. SPIE, 7459, Ocean
832 Remote Sensing: Methods and Applications, 74590G, doi: 10.1117/12.829251, 2009.

833 Dupouy, C., Loisel, H., Neveux, J., Brown, S. L., Moulin, C., Blanchot, J., Le Bouteiller, A.,
834 and Landry, M. R.: Microbial absorption and backscattering coefficients from in situ and
835 POLDER satellite data during an El Nino–Southern Oscillation cold phase in the equatorial
836 Pacific (180°), J. Geophys. Res., 108(C12), 8138, doi:10.1029/2001JC001298, 2003.
837 Dupouy, C., Neveux, J., and André, J. M.: Spectral absorption coefficient of
838 photosynthetically active pigments in the equatorial Pacific (165°E–150°W), Deep Sea
839 Res. Part II, 44, 1881–1906, 1997.
840 Dupouy, C., Neveux, J., Dirberg, G., Röttgers, R., Tenório, M. M. B., and Ouillon, S.: Bio-
841 optical properties of the marine cyanobacteria *Trichodesmium* spp, J. Appl. Remote Sens.,
842 2, 1–17, 2008.
843 Dupouy, C., Petit, M., and Dandonneau, Y.: Satellite detected cyanobacteria bloom in the
844 southwestern tropical Pacific. Implication for nitrogen fixation, Inter. J. Remote Sens., 8,
845 389–396, 1988.
846 Dupouy, C., Röttgers, R., Tedetti, M., Martias, C., Murakami, H., Doxaran, D., Lantoine, F.,
847 Rodier, M., Favareto, L., Kampel, M., Goutx, M., and Frouin, R.: Influence of CDOM and
848 Particle Composition on Ocean Color of the Eastern New Caledonia Lagoon during the
849 CALIOPE Cruises, Proc. of SPIE, 9261, Ocean Remote Sensing and Monitoring from
850 Space, 92610M, 2014.
851 Fellman, J. B., Hood, E., and Spencer, R. G. M.: Fluorescence spectroscopy opens new
852 windows into dissolved organic matter dynamics in freshwater ecosystems: A review,
853 Limnol. Oceanogr., 55, 2452–2462, 2010.
854 Foster, R. A., Subramaniam, A., and Zehr, J. P.: Distribution and activity of diazotrophs in the
855 Eastern Equatorial Atlantic, Environ. Microbiol., 11, 741–750, 2009.

Fuchs, R., Dupouy, C., Douillet, P., Caillaud, M., Mangin, A., Pinazo, C.: Modelling the impact of a La Niña event on a South West Pacific Lagoon, Mar. Pollut. Bull., 64, 1596–15613, 2012.

Grenz, C., Le Borgne, R., Fichez, R., and Torréton, J. P.: Tropical lagoon multidisciplinary investigations: An overview of the PNEC New Caledonia pilot site, Mar. Pollut. Bull., 61, 267–268, 2010.

Helms, J. R., Stubbins, A., Ritchie, J. D., Minor, E. C., Kieber, D. J., and Mopper, K.: Absorption spectral slopes and slope ratios as indicators of molecular weight, source and photobleaching of chromophoric dissolved organic matter, Limnol. Oceanogr., 53, 955–969, 2008.

Hernes, P. J., and Benner, R.: Terrigenous organic matter sources and reactivity in the North Atlantic Ocean and a comparison to the Arctic and Pacific oceans, Mar. Chem., 100, 66–79, 2006.

Ishii, S. K. L., and Boyer, T. H.: Behavior of Reoccurring PARAFAC Components in Fluorescent Dissolved Organic Matter in Natural and Engineered Systems: A Critical Review, Environ. Sci. Technol., 46, 2006–2017, 2012.

Kirchman, D. L., K'nees, E., and Hodson, R.: Leucine incorporation and its potential as a measure of protein synthesis by bacteria in natural waters, Appl. Environment. Microbiol., 49, 599–607, 1985.

Kowalczuk, P., Durako, M. J., Young, H., Kahn, A. E., Cooper, W. J., and Gonsior, M.: Characterization of dissolved organic matter fluorescence in the South Atlantic Bight with use of PARAFACmodel: interannual variability, Mar. Chem., 113, 182–196, 2009.

Kowalczuk, P., Tilstone, G. H., Zabłocka, M., Röttgers, R., and Thomas, R.: Composition of dissolved organic matter along an Atlantic Meridional Transect from fluorescence spectroscopy and Parallel Factor Analysis, Mar. Chem., 157, 170–184, 2013.

881 Lantoine, F., and Neveux, J.: Spatial and seasonal variations in abundance and spectral
882 characteristics of phycoerythrins in the tropical northeastern Atlantic Ocean, Deep-Sea
883 Res. I, 44, 223–246, 1997.
884 Le Bouteiller, A., Blanchot, J., and Rodier, M.: Size distribution patterns of phytoplankton in
885 the western Pacific: towards a generalization for the tropical open ocean, Deep Sea Res.
886 Part A. Oceanogr. Res. Pap., 39, 805–823, 1992.
887 Lefort, T., Gasol, J. M.: Short-time scale coupling of picoplankton community structure and
888 single-cell heterotrophic activity in winter in coastal NW Mediterranean Sea waters. J.
889 Plankton Res., 36, 243–258, 2014.
890 Lohrenz, S. E., Weidemann, A. D., and Tuel, M.: Phytoplankton spectral absorption as
891 influenced by community size structure and pigment composition, J. Plankton Res., 25,
892 35–61, 2003.
893 Lønborg, C., Yokokawa, T., Herndl, G. J., and Álvarez-Salgado, X. A.: Production and
894 degradation of fluorescent dissolved organic matter in surface waters of the eastern north
895 Atlantic ocean, Deep Sea Res. Part I, 96, 28–37.
896 Lutz, V. A., Sathyendranath, S., and Head, E. J. H.: Absorption coefficient of phytoplankton:
897 Regional variations in the North Atlantic, Mar. Ecol. Prog. Ser., 135, 197–213, 1996.
898 Lutz, V. A., Sathyendranath, S., Head, E., and Li, W. K. W: Changes in the in vivo absorption
899 and fluorescence excitation spectra with growth irradiance in three species of
900 phytoplankton. J. Plankton Res., 23, 555–569, 2001.
901 Marie, D., Partensky, F., Vaulot, D., and Brussaard, C. P. D.: Enumeration of phytoplankton,
902 bacteria, and viruses in marine samples. In Robinson, J. P., Darzynkiewicz, Z., Dean, P.
903 N., Orfao, A., Rabinovitch, P. S., Stewart, C. C., Tanke, H. J., Wheeless, L. L. (eds)
904 Current Protocols in Cytometry. John Wiley & Sons Inc., New York, pp. 11.11.1–
905 11.11.15, 1999.

Masotti, I., Ruiz Pino, D., and Le Bouteiller, A.: Photosynthetic characteristics of *Trichodesmium* in the southwest Pacific Ocean: importance and significance, Mar. Ecol. Progr. Ser., 338, 47–59, 2007.

Matsuoka, A., Babin, M., Doxaran, D., Hooker, S. B., Mitchell, B. G., Bélanger, S., and Bricaud, A.: A synthesis of light absorption properties of the Arctic Ocean: application to semianalytical estimates of dissolved organic carbon concentrations from space, Biogeosciences, 11, 3131–3147, 2014.

Morel, A.: Consequences of a *Synechococcus* bloom upon the optical properties of oceanic (case 1) waters, Limnol. Oceanogr., 42, 1746–1754, 1997.

Morel, A., Claustre, H., and Gentili, B.: The most oligotrophic subtropical zones of the global ocean: similarities and differences in terms of chlorophyll and yellow substance, Biogeosciences, 7, 3139–3151, 2010.

Morel, A., and Prieur, L.: Analysis of variations in ocean color, Limnol. Oceanogr., 22, 709–722, 1977.

Morel, A, Ahn, Y. H., Partensky, F., Vaulot, D., and Claustre, H.: *Prochlorococcus* and *Synechococcus* - A comparative study of their optical properties in relation to their size and pigmentation, J. Mar. Res. 51, 617–649, 1993.

Murphy, K. R., Stedmon, C. A., Waite, T .D., and Ruiz, G. M.: Distinguishing between terrestrial and autochthonous organic matter sources in marine environments using fluorescence spectroscopy, Mar. Chem., 108, 40–58, 2008.

Nagata, T.: Production mechanims of dissolved organic matter. In Kirchman, D. L. (ed.), Microbial Ecology of the Oceans. Wiley-Liss, New York, pp. 121–152, 2000.

Nelson, N. B., and Siegel, D. A.: The Global Distribution and Dynamics of Chromophoric Dissolved Organic Matter, Annu. Rev. Mar. Sci., 5, 447–476, 2013.

930 Nelson, N. B., Siegel, D. A., Carlson, C. A., and Swan, C. M.: Tracing global biogeochemical
931 cycles and meridional overturning circulation using chromophoric dissolved organic
932 matter, Geophys. Res. Lett. 37, L03610, 2010.
933 Nelson, N. B., Siegel, D. A., and Michaels, A. F.: Seasonal dynamics of colored dissolved
934 material in the Sargasso Sea, Deep-Sea Res. I, 45, 931–957, 1998.
935 Neveux, J., Lantoine, F., Vaulot, D., Marie, D., and Blanchot, J.: Phycoerythrins in the
936 southern tropical and equatorial Pacific Ocean: evidence for new cyanobacterial types, J.
937 Geophys. Res. 104, 3311–3321, 1999.
938 Neveux, J., Tenório, M. M. B., Jacquet, S., Torréton, J.-P., Douillet, P., Ouillon, S., Dupouy,
939 C.: Chlorophylls and Phycoerythrins as Markers of Environmental Forcings Including
940 Cyclone Erica Effect (March 2003) on Phytoplankton in the Southwest Lagoon of New
941 Caledonia and Oceanic Adjacent Area, Intern. J. Oceanogr., doi:10.1155/2009/232513,
942 2009.
943 Nieto-Cid, M., Álvarez-Salgado, X. A., and Pérez, F. F.: Microbial and photochemical
944 reactivity of fluorescent dissolved organic matter in a coastal upwelling system, Limnol.
945 Oceanogr., 51, 1391–1400, 2006.
946 Organelli, E., Bricaud, A., Antoine, D., and Matsuoka, A.: Seasonal dynamics of light
947 absorption by chromophoric dissolved organic matter (CDOM) in the NW Mediterranean
948 Sea (BOUSSOLE site), Deep-Sea Res. I, 91, 72–85, 2014.
949 Ortega-Retuerta, E., Frazer, T. K., Duarte, C. M., Ruiz-Halpern, S., Tovar-Sanchez, A.,
950 Arrieta, J. M., and Reche, I.: Biogeneration of chromophoric dissolved organic matter by
951 bacteria and krill in the Southern Ocean, Limnol. Oceanogr., 54, 1941–1950, 2009.
952 Ouillon, S., Douillet, P., Lefebvre, J. P., Le Gendre, R., Jouon, A., Bonneton, P., Fernandez, J.
953 M., Chevillon, C., Magand, O., Lefèvre, J., Le Hir, P., Laganier, R., Dumas, F.,
954 Marchesiello, P., Bel Madani, A., Andréfouët, S., Panché, J. Y., and Fichez, R.: Circulation

955 and suspended sediment transport in a coral reef lagoon: The south-west lagoon of New
956 Caledonia, Mar. Pollut. Bull., 61, 269–296, 2010.
957 Para, J., Coble, P. G., Charrière, B., Tedetti, M., Fontana, C., and Sempéré, R.: Fluorescence
958 and absorption properties of chromophoric dissolved organic matter (CDOM) in coastal
959 surface waters of the northwestern Mediterranean Sea, influence of the Rhône River,
960 Biogeosciences, 7, 4083-40103, 2010.
961 Pavlov, A. K., Silyakova, A., Granskog, M. A., Bellerby, R. G. J., Engel, A., Schulz, K. G.,
962 and Brussaard C. P. D.: Marine CDOM accumulation during a coastal Arctic mesocosm
963 experiment: No response to elevated pCO2 levels, J. Geophys. Res. Biogeosci., 119, 1216–
964 1230, doi:10.1002/2013JG002587, 2014.
965 Pujo-Pay, M., and Raimbault, P.: Improvement of the Wet-Oxidation Procedure for
966 Simultaneous Determination of Particulate Organic Nitrogen and Phosphorus Collected on
967 Filters, Mar. Ecol. Prog. Ser., 105, 203–207, 1994.
968 Rochelle-Newall, E., Delille, B., Frankignoulle, M., Gattuso, J. P., Jacquet, S., Riebesell, U.,
969 Terbrüggen A., and Zondervan, I.: Chromophoric dissolved organic matter in experimental
970 mesocosms maintained under different pCO2 levels, Mar. Ecol. Prog. Ser., 272, 25–31,
971 2004.
972 Rochelle-Newall, E. J., and Fisher, T. R.: Production of chromophoric dissolved organic
973 matter fluorescence in marine and estuarine environments: an investigation into the role of
974 phytoplankton, Mar. Chem., 77, 7–21, 2002.
975 Rochelle-Newall, E. J., Fisher, T. R., Fan, C., and Glibert, P. M.: Dynamics of chromophoric
976 dissolved organic matter and dissolved organic carbon in experimental mesocosms, Int. J.
977 Remote Sens. 20, 627– 641, 1999.

978 Rodier, M., and Le Borgne, R.: Population and trophic dynamics of *Trichodesmium thiebautii*
979 in the SE lagoon of New Caledonia. Comparison with *T. erythraeum* in the SW lagoon,
980 Mar. Pollut. Bull., 61, 349–359, 2010.
981 Romera-Castillo, C., Sarmento, H., Álvarez-Salgado, X. A., Gasol, J. M., and Marrasé, C.:
982 Production of chromophoric dissolved organic matter by marine phytoplankton, Limnol.
983 Oceanogr., 55, 446–454, 2010.
984 Romera-Castillo, C., Sarmento, H., Álvarez-Salgado, X. A., Gasol, J. M., and Marrasé, C.:
985 Net Production and Consumption of Fluorescent Colored Dissolved Organic Matter by
986 Natural Bacterial Assemblages Growing on Marine Phytoplankton Exudates, Appl.
987 Environment. Microbiol., 77, 7490–7498, 2011.
988 Röttgers, R., and Doerffer, R.: Measurements of optical absorption by chromophoric
989 dissolved organic matter using a point-source integrating-cavity absorption meter, Limnol.
990 Oceanogr. Met., 126–135, 2007.
991 Röttgers, R., Dupouy, C., Taylor, B. B., Bracher, A., and Wozniak, S. B.: Mass-specific light
992 absorption coefficients of natural aquatic particles in the near-infrared spectral region,
993 Limnol. Oceanogr., 59, 1449–1460, 2014.
994 Röttgers, R., Häse, C., and Doerffer, R.: Determination of the particulate absorption of
995 microalgae using a point-source integrating-cavity absorption meter: verification with a
996 photometric technique, improvements for pigment bleaching and correction for chlorophyll
997 fluorescence, Limnol. Oceanogr. Methods, 5, 1–12, 2007.
998 Röttgers, R., and Koch, B. P.: Spectroscopic detection of a ubiquitous dissolved pigment
999 degradation product in subsurface waters of the global ocean, Biogeosciences, 9, 2585–
1000 2596, 2012.

1001 Sempéré, R., Para, J., Tedetti, M., Charrière, B., and Mallet, M.: Variability of solar radiation
1002 and CDOM in surface coastal waters of the Northwestern Mediterranean Sea. Photochem.
1003 Photobiol., 91, 851–861, 2015.
1004 Siegel, D. A., Maritorena, S., Nelson, N. B., and Behrenfeld, M. J.: Independence and
1005 interdependencies of global ocean color properties; Reassessing the bio-optical
1006 assumption, J. Geophys. Res., 110, C07011, doi:10.1029/2004JC002527, 2005.
1007 Siegel, D. A., Maritorena, S., Nelson, N. B., Hansell, D. A., and Lorenzi-Kayser, M.: Global
1008 distribution and dynamics of colored dissolved and detrital organic materials, J. Geophys.
1009 Res., 107(C12), 3228, doi:10.1029/2001JC000965, 2002.
1010 Smith, D. C, and Azam, F.: A simple, economical method for measuring bacterial protein
1011 synthesis rates in sea water using 3H-Leucine, Mar. Microb. Food Webs, 6, 107–114,
1012 1992.
1013 Sohrin, R., and Sempéré R.: Temporal variation in total organic carbon in the Northeast
1014 Atlantic in 2000–2001, J. Geophys. Res. 110, C10S90, doi: 10.1029/2004JC002731, 2005.
1015 Stedmon, C. A., and Bro, R.: Characterizing dissolved organic matter fluorescence with
1016 parallel factor analysis: a tutorial, Limnol. Oceanogr. Met., 6, 572–579, 2008.
1017 Stedmon, C. A., and Cory, R. M.: Biological Origins and Fate of Fluorescent Dissolved
1018 Organic Matter in Aquatic Environments. In Aquatic Organic Matter Fluorescence. Eds
1019 PG Coble, J Lead, A. Baker, DM Reynolds, RGM Spencer.Cambridge University Press,
1020 New York, pp. 278–299, 2014.
1021 Stedmon, C. A., Markager, S., and Bro, R.: Tracing dissolved organic matter in aquatic
1022 environments using a new approach to fluorescence spectroscopy, Mar. Chem., 82, 239–
1023 254, 2003.

1024 Steinberg, D. K., Nelson, N., Carlson, C. A., and Prusak, A. C.: Production of chromophoric
1025 dissolved organic matter (CDOM) in the open ocean by zooplankton and the colonial
1026 cyanobacterium *Trichodesmium* spp, Mar. Ecol. Prog. Ser., 267, 45–56, 2004.
1027 Stramski, D., and Mobley, C. D.: Effects of microbial particles on oceanic optics: A database
1028 of single-particle optical properties. Limnol. Oceanogr., 42, 538–549, 1997.
1029 Stuart, V., Sathyendranath, S., Platt, T., Maass, H., and Irwin, B. D.: Pigment and species
1030 composition of natural phytoplankton populations: Effect on the absorption spectra, J.
1031 Plankton Res., 20, 187–217, 1998.
1032 Subramaniam, A., Carpenter, E. J., Karentz, D., and Falkowski, P. G.: Bio-optical properties
1033 of the marine diazotrophic cyanobacteria *Trichodesmium* spp. I. Absorption and
1034 photosynthetic action spectra, Limnol. Oceanogr., 44, 608–617, 1999.
1035 Swan, C., M., Siegel, D. A., Nelson, N. B., Carlson, C. A., and Nasir, E.: Biogeochemical and
1036 hydrographic controls on chromophoric dissolved organic matter distribution in the Pacific
1037 Ocean, Deep-Sea Res. I Oceanogr. Res. Pap., 56, 2175–2192, 2009.
1038 Swan, C. M., Siegel, D. A., Nelson, N. B., and Kostadinov, T. S.: The effect of surface
1039 irradiance on the absorption spectrum of chromophoric dissolved organic matter in the
1040 global ocean, Deep-Sea Res. I, 63, 52–64, 2012.
1041 Tedetti, M., Charrière, B., Bricaud, A., Para, J., Raimbault, P., and Sempéré, R.: Distribution
1042 of normalized waterleaving radiances at UV and visible wave bands in relation with
1043 chlorophyll a and colored detrital matter content in the southeast Pacific, J. Geophys. Res.,
1044 115, C02010, doi:10.1029/2009JC005289, 2010.
1045 Tedetti, M., Longhitano, R., Garcia, N., Guigue, C., Ferretto, N., and Goutx, M.: Fluorescence
1046 properties of dissolved organic matter in coastal Mediterranean waters influenced by a
1047 municipal sewage effluent (Bay of Marseilles, France), Environ. Chem., 9, 438–449, 2012.

1048 Tedetti, M., Sempéré, R., Vasilkov, A., Charrière, B., Nérini, D., Miller, W., Kawamura, K.,
1049 and Raimbault, P.: High penetration of ultraviolet radiation in the south east Pacific waters,
1050 Geophys. Res. Lett., 34, L12610, doi:10.1029/2007 GL029823, 2007.
1051 Tilstone, G. H., Peters, S. W. M., van derWoerd, H. J., Eleveld, M. A., Ruddick, K.,
1052 Schönfeld, W., Krasemann, H., Martinez-Vicente, V., Blondeau-Patissier, D., Röttgers, R.,
1053 Sørensen, K., Jørgenseng, P. V., and Shutler, J. D.: Variability in specific-absorption
1054 properties and their use in a semianalytical ocean colour algorithm for MERIS in north sea
1055 andwestern English channel coastal waters, Remote Sen. Environ., 118, 320–338, 2012.
1056 Turk-Kubo, K. A., Frank, I. E., Hogan, M. E., Desnues, A., Bonnet, S., and Zehr, J. P.:
1057 Diazotroph community succession during the VAHINE mesocosms experiment (New
1058 Caledonia Lagoon), Biogeosciences, 12, 7435–7452, 2015.
1059 Twardowski, M. S., Boss, E., Sullivan, J. M., and Donaghay, P. L.: Modeling the spectral
1060 shape of absorption by chromophoric dissolved organic matter, Mar. Chem., 89, 69–88,
1061 2004.
1062 Vernet, M., and Whitehead, K.: Release of ultraviolet-absorbing compounds by the red-tide
1063 dinoflagellate *Lingulodinium polyedra*, Mar. Biol., 127, 35–44, 1996.
1064 Whitehead, K., and Vernet, M.: Influence of mycosporine-like amino acids (MAAs) on UV
1065 absorption by particulate and dissolved organic matter in La Jolla Bay, Limnol. Oceanogr.,
1066 45,1788–1796, 2000.
1067 Wyman, M.: An in vivo method for the estimation of phycoerythrin concentrations in marine
1068 cyanobacteria (Synechococcus spp.), Limnol. Oceanogr., 37, 1300–1306, 1992.
1069 Wozniak, B., Dera, J., Ficek, D., Machrowski, R., Kaczmarek, S., Ostrowska, M., and
1070 Koblentz-Mischke, O. I.: Modelling the influence of acclimation on the absorption
1071 properties of marine phytoplankton, Oceanologia, 41, 187–210, 1999.

Xing, X., Claustre, H., Wang, H., Poteau, A., and D'Ortenzio, F.: Seasonal dynamics in colored dissolved organic matter in the Mediterranean Sea: patterns and drivers, Deep-Sea Res. I, 83, 93–101, 2014.

Yamashita, Y., Jaffe, R., Maie, N., and Tanoue, E.: Assessing the dynamics of dissolved organic matter (DOM) in coastal environments by excitation emission matrix fluorescence and parallel factor analysis (EEM-PARAFAC), Limnol. Oceanogr., 53, 1900−1908, 2008.

Yamashita, Y., Nosaka, Y., Suzuki, K., Ogawa, H., Takahashi, K., and Saito H: Photobleaching as a factor controlling spectral characteristics of chromophoric dissolved organic matter in open ocean, Biogeosciences, 10, 7207–7217, 2013.

Yamashita, Y., Tanoue, E.: In situ production of chromophoric dissolved organic matter in coastal environments, Geophys. Res. Lett., 31(14), 1–4. doi:10.1029/2004GL019734, 2004.

Figure captions

Figure 1. Location of the site of the VAHINE mesocosm experiment at the exit of the New Caledonian coral lagoon, 28 km off the coast of New Caledonia, in the South West Pacific (Ocean Data View software version 4.6.5, Schlitzer, R., http://odv.awi.de, 2014, and Google Earth).

Figure 2. Pictures of the VAHINE mesocosms deployed at the exit of the New Caledonian coral lagoon.

Figure 3. Evolution of a) total chlorophyll *a* (TChl *a*) and b) phycoerythrin concentrations ($\mu g\ L^{-1}$), c) total organic carbon (TOC), d) particulate organic nitrogen (PON) and e) dissolved organic nitrogen (DON) concentrations (μM) and f) bacterial production (BP) (ng C $L^{-1}\ h^{-1}$) in the mesocosm M1 and in the surrounding waters (OUT) at 1, 6 and 12 m depths (except phycoerythrin and TOC concentrations, determined only at 6 m depth) over the course of the 23-day experiment. Dots are mean values with standard deviation from duplicate measurements, except for phycoerythrin. For TChl *a*, standard deviations are comprised within dots. Black line represents the depth-averaged values. P1: first part of the experiment, from day 5 to day 14; P2: second part of the experiment, from day 15 to day 23.

Figure 4. Evolution of the abundance of a) diatoms-diazotrophs associations (DDAs) and b) unicellular diazotrophic cyanobacteria Group C (UCYN-C) ($\times 10^3$ *nifH* copies L^{-1}) in the mesocosm M1 and in the surrounding waters (OUT), and c) total diatoms ($\times 10^3$ cell L^{-1}), d) *Synechoccocus* spp., e) *Prochloroccocus* spp., f) picoeukaryotes and g) nanoeukaryotes ($\times 10^3$ cell mL^{-1}) in the mesocosm M1 only, over the course of the 23-day experiment.

Synechoccocus spp., *Prochloroccocus* spp., picoeukaryotes and nanoeukaryotes were determined at 1, 6 and 12 m depths, while DDAs, UCYN-C and total diatoms were determined solely at 6 m depth. For DDAs and UCYN-C, dots are mean values with standard deviation from duplicate measurements. Black line represents the depth-averaged values. P1: first part of the experiment, from day 5 to day 14; P2: second part of the experiment, from day 15 to day 23. Detailed data about diazotrophs (DDAs and UCYN-C) are found in Turk-Kubo et al. (2015).

Figure 5. Absorption spectra of chromophoric dissolved organic matter (CDOM) and particulate matter over the ranges 370-720 nm of samples collected in the mesocosm M1 at 1, 6 and 12 m depths and in the surrounding waters at 1 m depth. Black lines represent the average of all spectra and shaded areas represent the measured minimal and maximal values. Peaks and shoulders are reported for particulate matter.

Figure 6. Evolution of a) absorption coefficient of CDOM at 370 nm [$a_g(370)$ in m^{-1}], b) absorption coefficient of CDOM at 442 nm [$a_g(442)$ in m^{-1}], c) spectral slope of CDOM absorption in the range 370-500 nm (S_g in nm^{-1}), d) absorption coefficient of particulate matter at 442 nm [$a_p(442)$ in m^{-1}] and e) absorption coefficient of particulate matter at 676 nm [$a_p(676)$ in m^{-1}] in the mesocosm M1 at 1, 6 and 12 m depths and in the surrounding waters (OUT) at 1 m depth over the course of the 23-day experiment. Dots are mean values with standard deviation from duplicate measurements, except for S_g. Black line represents the depth-averaged values. P1: first part of the experiment, from day 5 to day 14; P2: second part of the experiment, from day 15 to day 23.

Figure 7. Spectral characteristics of the three FDOM components (C1-C3) validated by the PARAFAC model for 130 EEMs of samples collected in the mesocosm M1 at 1, 6 and 12 m depths and in the surrounding waters at 1 m depth over the course of the 23-day experiment. Both contour (left column) and line (right column) plots are depicted. The line plots show the excitation (left side) and emission (right side) fluorescence spectra. The dotted grey lines correspond to split half validation results. The excitation and emission maxima (λ_{Ex} and λ_{Em}) of each component are given.

Figure 8. Evolution of the fluorescence intensities (QSU) of the three FDOM components: a) humic-like, b) tryptophan-like and c) tyrosine-like fluorophores in the mesocosm M1 at 1, 6 and 12 m depths over the course of the 23-day experiment (actually up to day 20 and not to day 23). Dots are mean values with standard deviation from duplicate measurements. Black line represents the depth-averaged values. P1: first part of the experiment, from day 5 to day 14; P2: second part of the experiment, from day 15 to day 23. Fluorescence intensities in the surrounding waters (OUT) at 1 m depth were determined on only few samples at the beginning and the end of the experiment and are thus not presented here.

Figure 9. Linear relationships between absorption coefficient of CDOM at 370 nm [$a_g(370)$ in m^{-1}] or absorption coefficient of particulate matter at 442 nm [$a_p(442)$ in m^{-1}] and *Synechoccocus* spp. abundance ($\times 10^3$ cell mL^{-1}) for samples collected in the mesocosm M1 from day 5 to day 20, i.e. from the day after the dissolved inorganic phosphorus fertilization to almost the end of the experiment (P1 + P2) (n = 36).

Table 1. Mean values and associated standard deviations of chromophoric, biogeochemical and biological parameters of samples collected in the mesocosm M1 and in the surrounding waters (OUT) during the first part of the experiment, i.e. from day 5 to day 14 (P1), and during the second part of the experiment, i.e. from day 15 to day 23 (P2). The means which have different letters (*a*, *b*, *c* or *d*) are significantly different (ANOVA, $p < 0.05$). M1-P2 values in bold are significantly different from M1-P1, OUT-P1 and OUT-P2 values.

	M1-P1 (*n*)	M1-P2 (*n*)	OUT-P1 (*n*)	OUT-P2 (*n*)
TChl *a* (µg L^{-1})	0.19 ± 0.05^{a} (28)	**0.42 ± 0.14^{b}** (27)	0.21 ± 0.03^{a} (25)	0.30 ± 0.07^{c} (25)
Phycoerythrin (µg L^{-1})	0.17 ± 0.09^{a} (9)	0.24 ± 0.09^{a} (9)	0.19 ± 0.08^{a} (10)	0.42 ± 0.19^{b} (9)
TOC (µM)	66.5 ± 2.1^{a} (9)	69.7 ± 4.3^{b} (9)	66.6 ± 2.8^{a} (9)	$67.7 \pm 1.5^{a,b}$ (7)
PON (µM)	0.81 ± 0.13^{a} (30)	**1.10 ± 0.21^{b}** (27)	0.71 ± 0.06^{c} (30)	0.87 ± 0.13^{a} (27)
DON (µM)	5.5 ± 1.4^{a} (29)	4.8 ± 0.6^{a} (22)	5.0 ± 0.4^{a} (29)	5.3 ± 1.8^{a} (23)
BP (ng C L^{-1} h^{-1})	157 ± 49^{a} (30)	**348 ± 142^{b}** (27)	135 ± 24^{a} (30)	256 ± 60^{c} (27)
DDAs (× 10^3 *nifH* copies L^{-1})	$120 \pm 45^{a,b}$ (5)	54 ± 31^{a} (6)	$227 \pm 189^{b,c}$ (5)	$200 \pm 220^{a,c}$ (3)
UCYN-C (× 10^3 *nifH* copies L^{-1})	4.5 ± 7.6^{a} (4)	**64 ± 24^{b}** (6)	1.2 ± 0.8^{a} (5)	2.9 ± 1.7^{a} (3)
Total diatoms (× 10^3 cell L^{-1})	17 ± 9^{a} (5)	44 ± 37^{a} (5)	*nd*	*nd*
Synechococcus (× 10^3 cell mL^{-1})	41 ± 20^{a} (24)	**88 ± 14^{b}** (23)	*nd*	*nd*
Prochlorococcus (× 10^3 cell mL^{-1})	12 ± 6^{a} (24)	15 ± 3^{a} (23)	*nd*	*nd*
Picoeukaryotes (× 10^3 cell mL^{-1})	1.5 ± 0.8^{a} (24)	**2.4 ± 0.6^{b}** (23)	*nd*	*nd*
Nanoeukaryotes (× 10^3 cell mL^{-1})	0.9 ± 0.4^{a} (24)	**1.5 ± 0.4^{b}** (23)	*nd*	*nd*
$a_g(370)$ (m^{-1})	0.046 ± 0.004^{a} (30)	**0.058 ± 0.009^{b}** (27)	$0.049 \pm 0.005^{a,c}$ (9)	0.052 ± 0.006^{c} (9)
$a_g(442)$ (m^{-1})	0.013 ± 0.001^{a} (30)	0.016 ± 0.003^{b} (27)	$0.015 \pm 0.002^{a,c}$ (9)	$0.015 \pm 0.001^{c,b}$ (9)
S_g (nm^{-1})	$0.0172 \pm 0.001^{a,b}$ (30)	0.0174 ± 0.001^{b} (27)	0.0169 ± 0.001^{a} (9)	0.0169 ± 0.001^{a} (9)
$a_p(442)$ (m^{-1})	0.014 ± 0.004^{a} (30)	**0.022 ± 0.004^{b}** (27)	0.015 ± 0.002^{a} (9)	0.018 ± 0.002^{c} (9)
$a_p(676)$ (m^{-1})	0.005 ± 0.002^{a} (30)	0.009 ± 0.002^{b} (27)	0.005 ± 0.001^{a} (9)	0.008 ± 0.001^{b} (9)
Humic-like (QSU)	4.47 ± 0.76^{a} (30)	4.45 ± 1.09^{a} (18)	*nd*	*nd*
Tryptophan-like (QSU)	7.68 ± 1.17^{a} (30)	8.07 ± 2.07^{a} (18)	*nd*	*nd*
Tyrosine-like (QSU)	6.57 ± 1.21^{a} (28)	**5.49 ± 0.83^{b}** (18)	*nd*	*nd*

nd: not determined; TChl *a*: total chlorophyll *a* concentration; TOC: total organic carbon concentration; PON and DON: particulate and dissolved organic nitrogen concentrations; BP: bacterial production; DDAs: diatoms-diazotrophs associations; UCYN-C: unicellular diazotrophic cyanobacteria Group C; $a_g(370)$ and $a_g(442)$: absorption coefficients of CDOM at 370 and 442 nm; S_g: spectral slope of CDOM; $a_p(442)$ and $a_p(676)$: absorption coefficients of

particulate matter at 442 and 676 nm; Humic-like, tryptophan-like and tyrosine-like: fluorescence intensity of humic-like, tryptophan-like and tyrosine-like FDOM fluorophores. Detailed data about diazotrophs (DDAs and UCYN-C) are found in Turk-Kubo et al. (2015).

Table 2. Pearson's correlation coefficients (*r*) of linear regressions between the chromophoric and the biogeochemical/biological parameters of samples collected in the mesocosm M1 from day 5 to day 20, i.e. from the day after the dissolved inorganic phosphorus fertilization to almost the end of the experiment (P1 + P2) (n = 36).

	$a_g(370)$	$a_g(442)$	S_g	$a_p(442)$	$a_p(676)$	Humic	Trypto.	Tyrosine
$a_g(442)$	**0.90**							
S_g	0.22	-0.15						
$a_p(442)$	**0.61**	0.52	0.23					
$a_p(676)$	**0.62**	0.53	0.30	**0.93**				
Humic	0.42	0.36	0.13	0.22	0.10			
Trypto.	0.28	0.24	0.28	0.17	0.16	**0.67**		
Tyrosine	-0.09	-0.25	0.11	-0.28	-0.39	0.48	0.20	
TChl *a*	**0.68**	**0.60**	0.32	**0.86**	**0.88**	0.22	0.21	-0.33
Phyco.*	0.45	0.42	0.11	0.74	0.73	0.05	0.00	-0.35
TOC*	0.35	0.16	0.63	0.57	0.59	0.52	0.43	0.28
PON	**0.71**	**0.58**	0.29	**0.75**	**0.70**	0.43	0.29	0.04
DON	-0.30	-0.23	-0.13	-0.14	-0.04	-0.26	-0.10	-0.14
BP	**0.75**	**0.72**	0.10	**0.78**	**0.72**	0.43	0.32	-0.12
DDAs*	-0.44	-0.38	-0.52	-0.85	-0.78	0.20	0.05	0.60
UCYN-C*	0.73	0.67	0.55	0.90	0.85	0.15	0.23	-0.47
Diatoms*	-0.07	-0.08	0.40	0.49	0.47	-0.85	-0.74	-0.88
Synecho.	**0.76**	**0.76**	0.08	**0.83**	**0.76**	0.35	0.29	-0.27
Prochlo.	0.42	0.47	0.08	0.57	0.50	0.13	0.03	0.00
Picoeuka.	0.52	**0.62**	-0.07	**0.71**	**0.58**	0.40	0.34	-0.25
Nanoeuka.	0.48	0.45	0.01	**0.65**	**0.58**	0.11	0.01	-0.35

Correlation coefficients (*r*) in bold are very highly significant ($p < 0.0001$). * Correlations determined on a lower number of samples (*n*): 15 for Phyco. and TOC, 10 for DDAs, 9 for UCYN-C and 8 for diatoms. $a_g(370)$ and $a_g(442)$: absorption coefficients of CDOM at 370 and 442 nm (m^{-1}); S_g: spectral slope of CDOM; $a_p(442)$ and $a_p(676)$: absorption coefficients of particulate matter at 442 and 676 nm (m^{-1}); Humic: fluorescence intensity of humic-like fluorophore (QSU); Trypto.: fluorescence intensity of tryptophan-like fluorophore (QSU); Tyrosine: fluorescence intensity of tyrosine-like fluorophore (QSU); TChl *a*: total chlorophyll *a* concentration ($\mu g\ L^{-1}$); Phyco.: phycoerythrin concentration ($\mu g\ L^{-1}$); TOC: total organic carbon concentration (μM); PON and DON: particulate and dissolved organic nitrogen concentrations (μM); BP: bacterial production (ng C L^{-1} h^{-1}); DDAs: diatoms-diazotrophs associations (*nifH* copies L^{-1}); UCYN-C: unicellular diazotrophic cyanobacteria Group C (*nifH*

copies L^{-1}); Diatoms: total diatoms (cell L^{-1}); *Synecho*.: *Synechococcus* spp. (cell mL^{-1}); *Prochlo*.: *Prochlorococcus* spp. (cell mL^{-1}); Picoeuka.: Picoeukaryote (cell mL^{-1}); Nanoeuka.: Nanoeukaryote (cell mL^{-1}). Detailed data about diazotrophs (DDAs and UCYN-C) are found in Turk-Kubo et al. (2015).

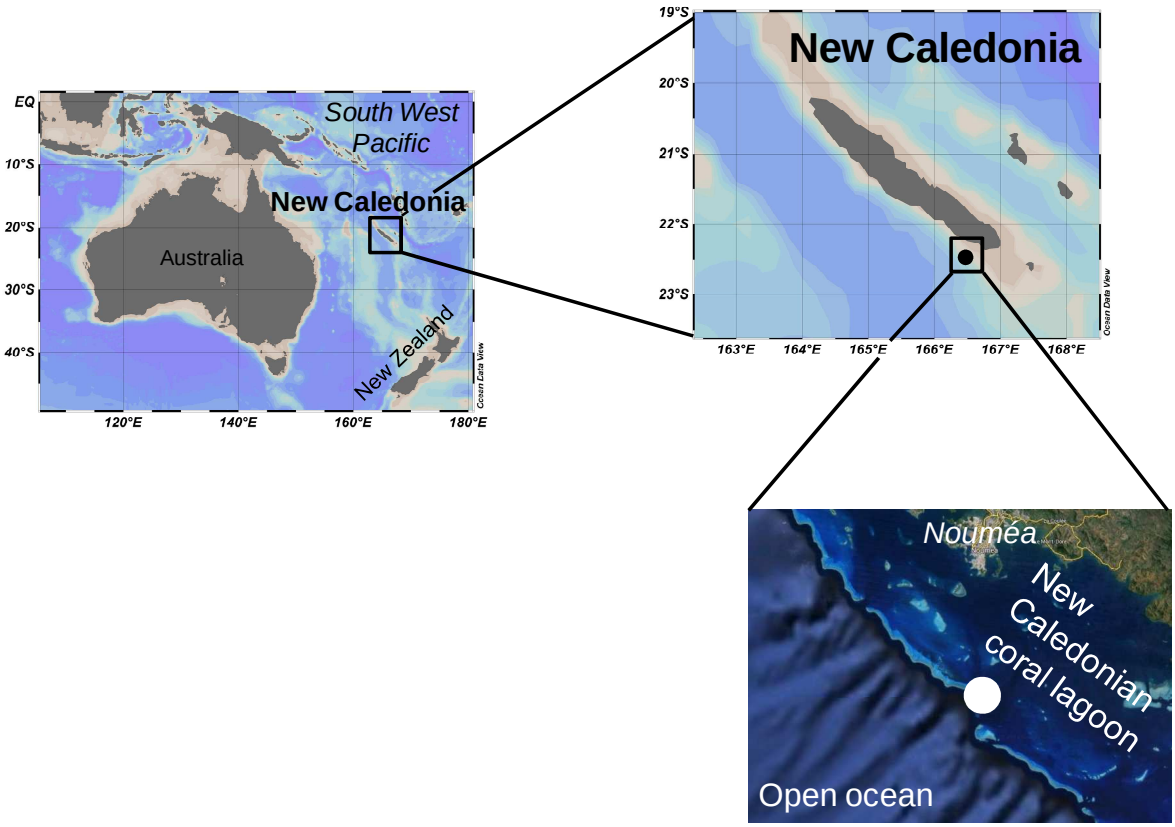
South West Pacific
New Caledonia
Australia
New Zealand
EQ
10°S
20°S
30°S
40°S
120°E
140°E
160°E
180°E
Ocean Data View
New Caledonia
19°S
20°S
21°S
22°S
23°S
163°E
164°E
165°E
166°E
167°E
168°E
Ocean Data View
Nouméa
New Caledonian coral lagoon
Open ocean

Figure 1

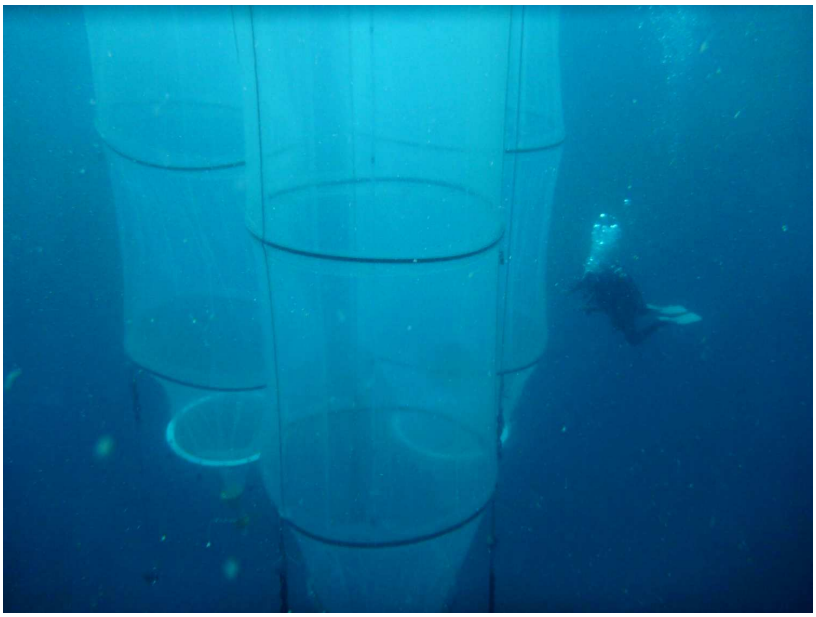

Figure 2

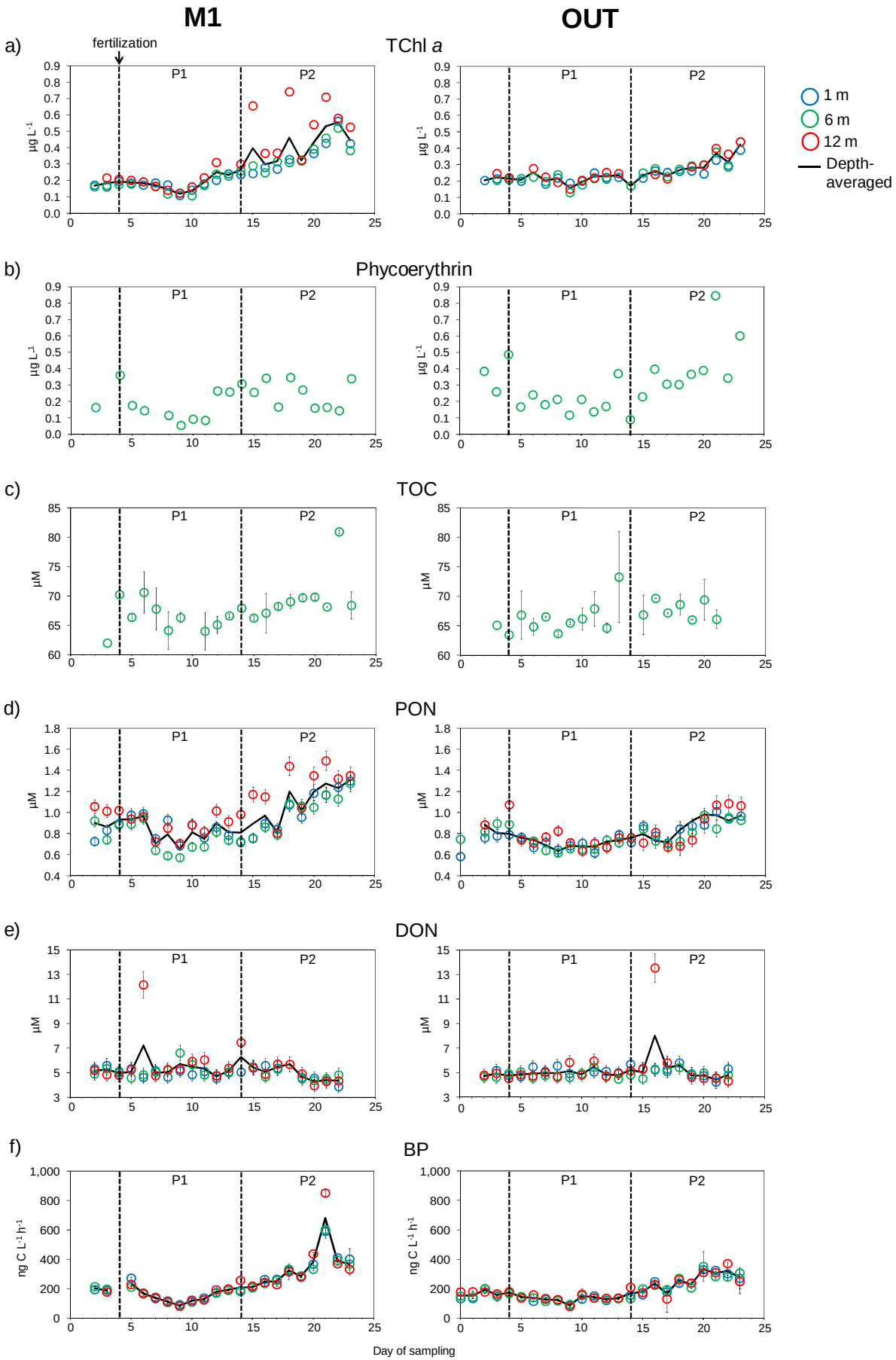

1282 Figure 3

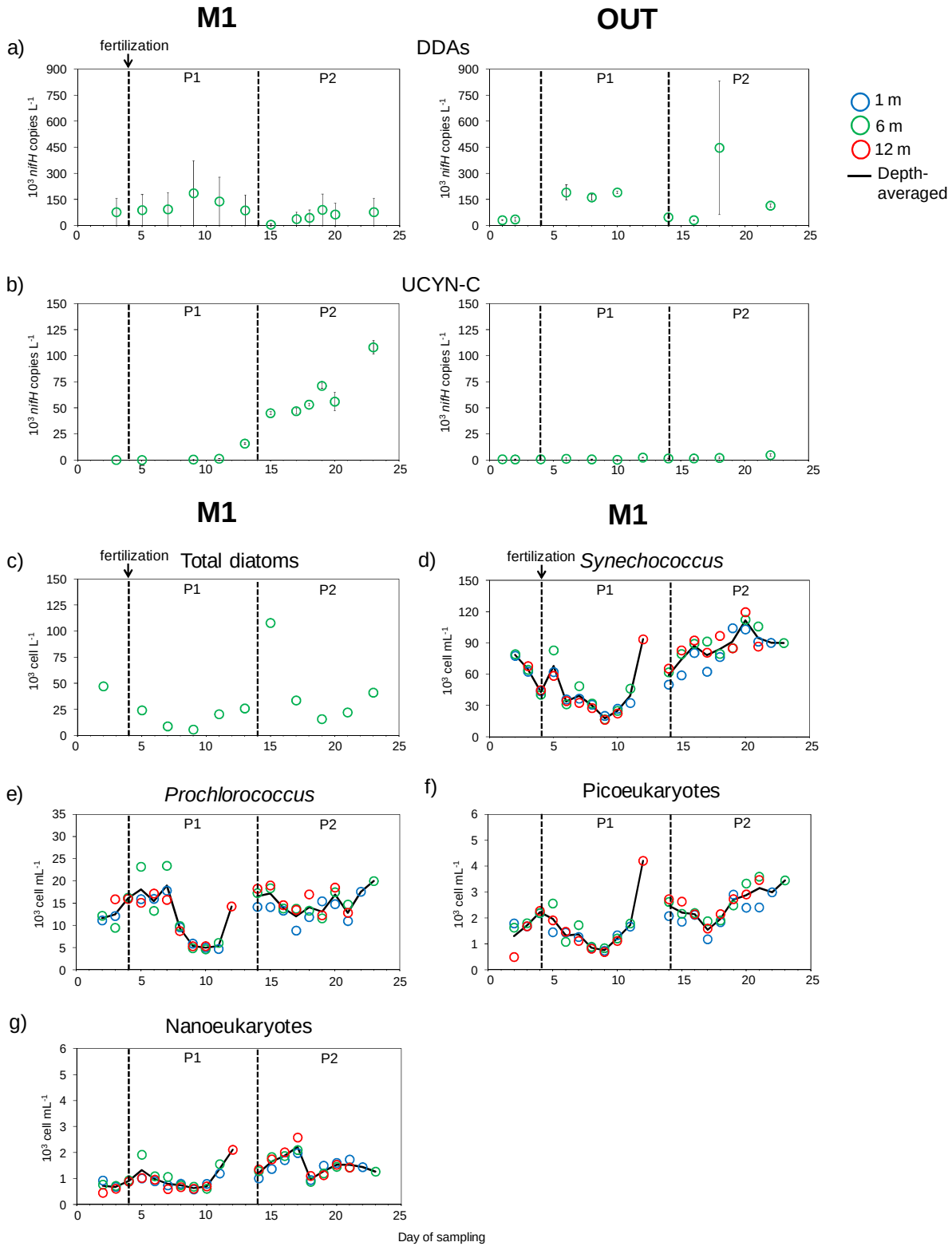
M1
OUT
a)
fertilization
DDAs
P1
P2
10³ nifH copies L⁻¹
1 m
6 m
12 m
Depth-averaged
b)
UCYN-C
M1
M1
c)
Total diatoms
10³ cell L⁻¹
d)
Synechococcus
10³ cell mL⁻¹
e)
Prochlorococcus
f)
Picoeukaryotes
g)
Nanoeukaryotes
Day of sampling

Figure 4

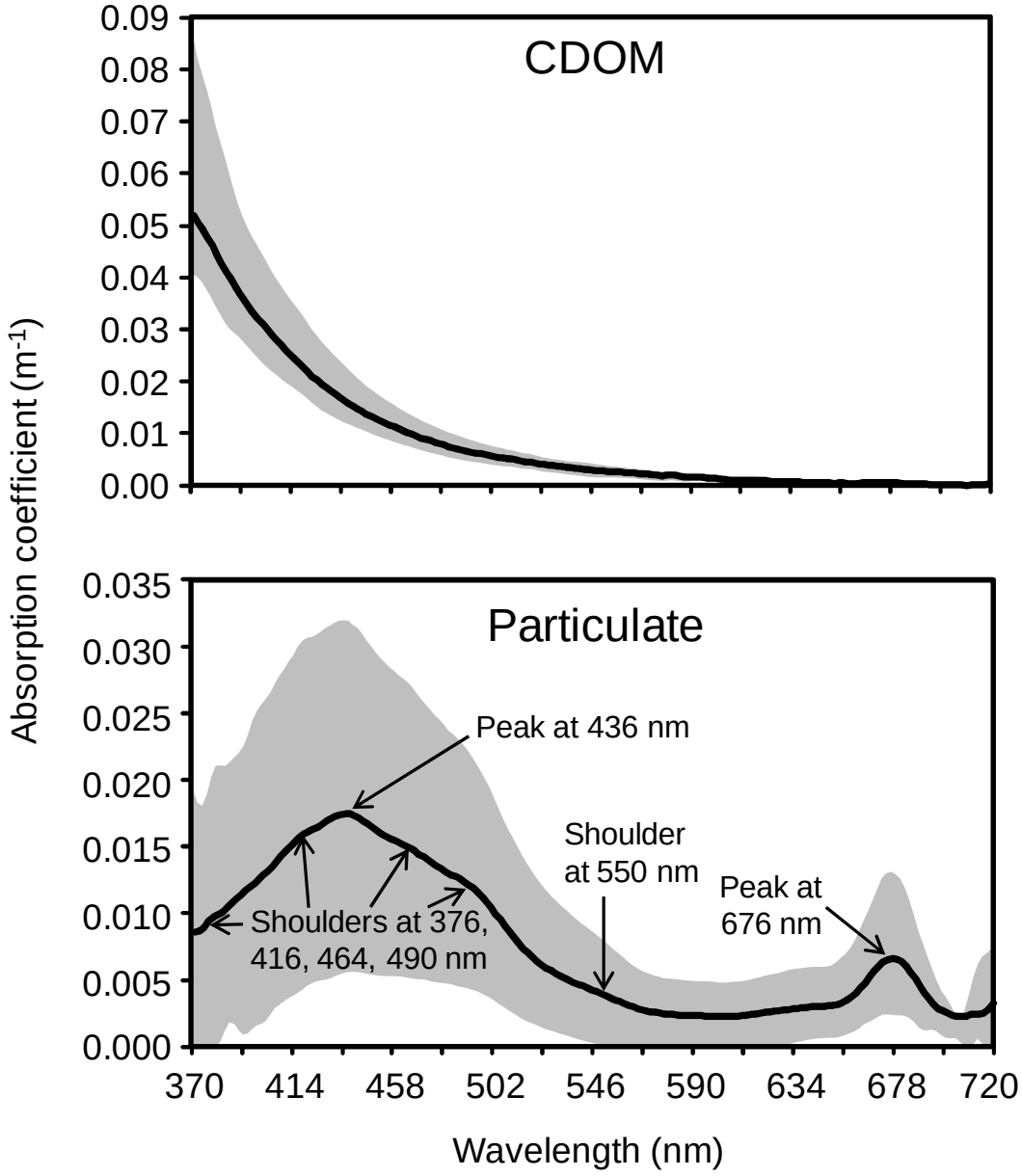
CDOM
Particulate
Absorption coefficient (m-1)
0.09
0.08
0.07
0.06
0.05
0.04
0.03
0.02
0.01
0.00
0.035
0.030
0.025
0.020
0.015
0.010
0.005
0.000
Peak at 436 nm
Shoulder
at 550 nm
Peak at
676 nm
Shoulders at 376,
416, 464, 490 nm
370
414
458
502
546
590
634
678
720
Wavelength (nm)

Figure 5

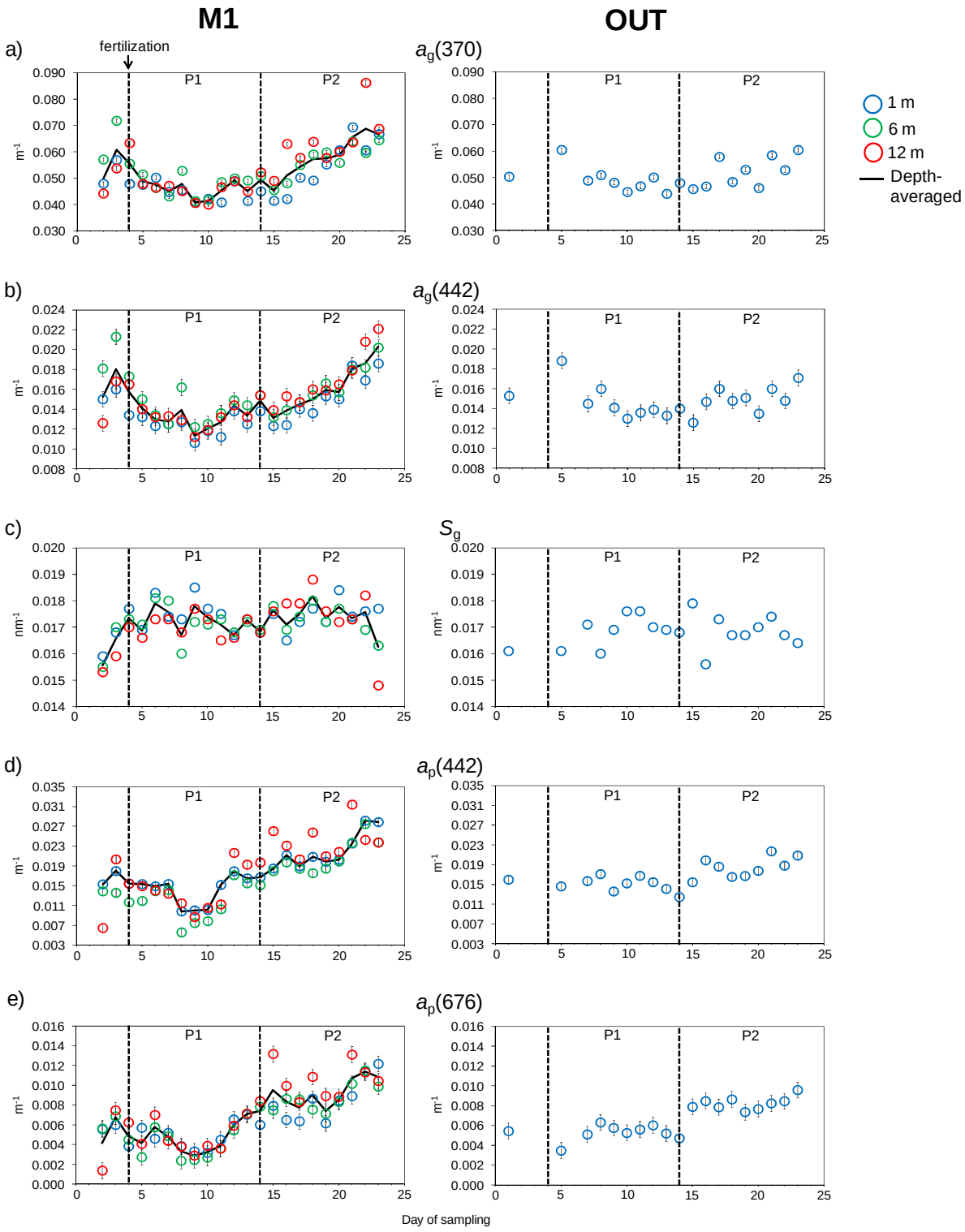
M1
OUT
a)
fertilization
a_g(370)
b)
a_g(442)
c)
S_g
d)
a_p(442)
e)
a_p(676)
P1
P2
m⁻¹
nm⁻¹
1 m
6 m
12 m
Depth-averaged
Day of sampling

Figure 6

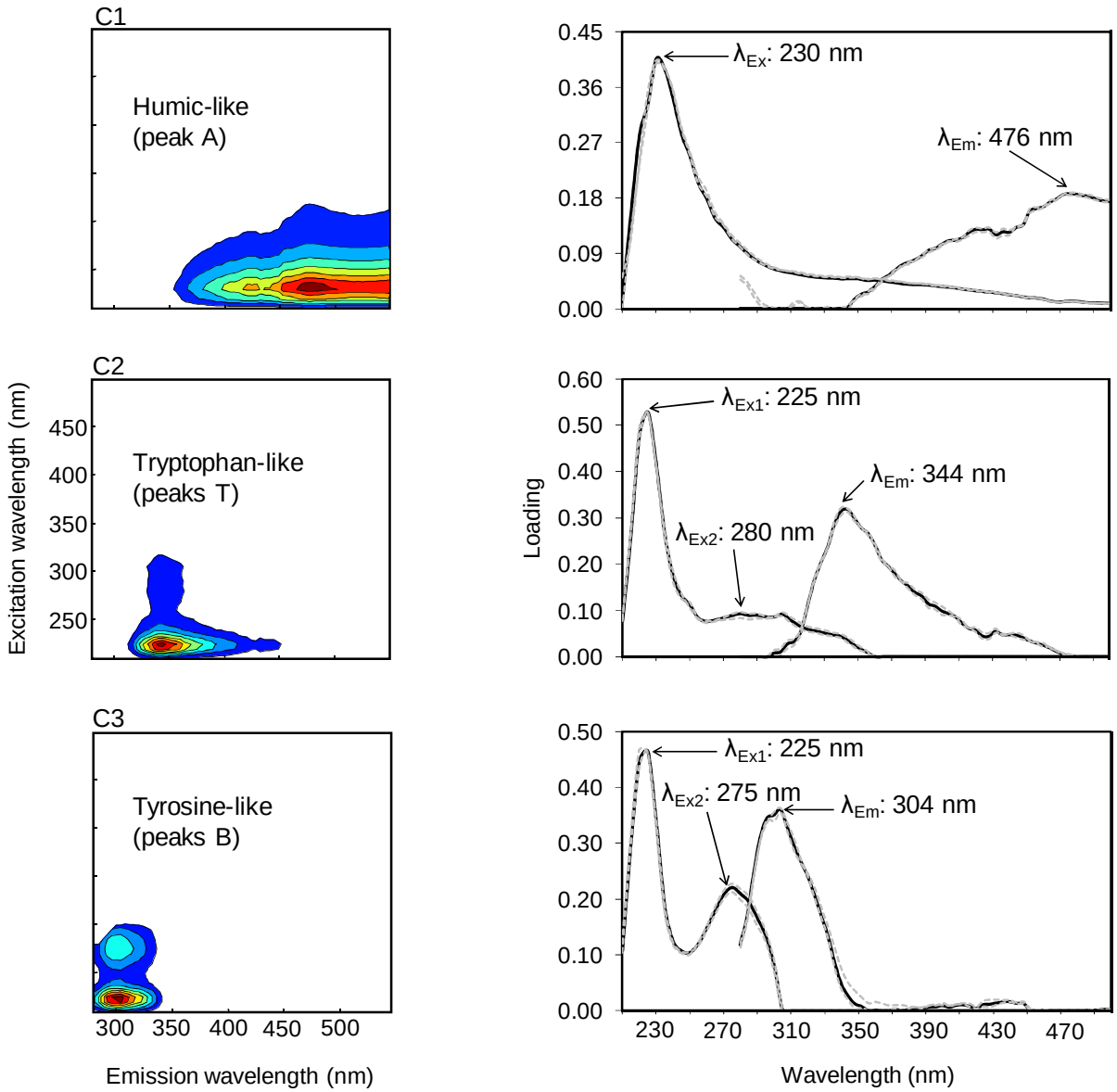
C1
Humic-like
(peak A)
λEx: 230 nm
λEm: 476 nm
C2
Tryptophan-like
(peaks T)
λEx1: 225 nm
λEm: 344 nm
λEx2: 280 nm
C3
Tyrosine-like
(peaks B)
λEx1: 225 nm
λEx2: 275 nm
λEm: 304 nm
Excitation wavelength (nm)
Emission wavelength (nm)
Loading
Wavelength (nm)

Figure 7

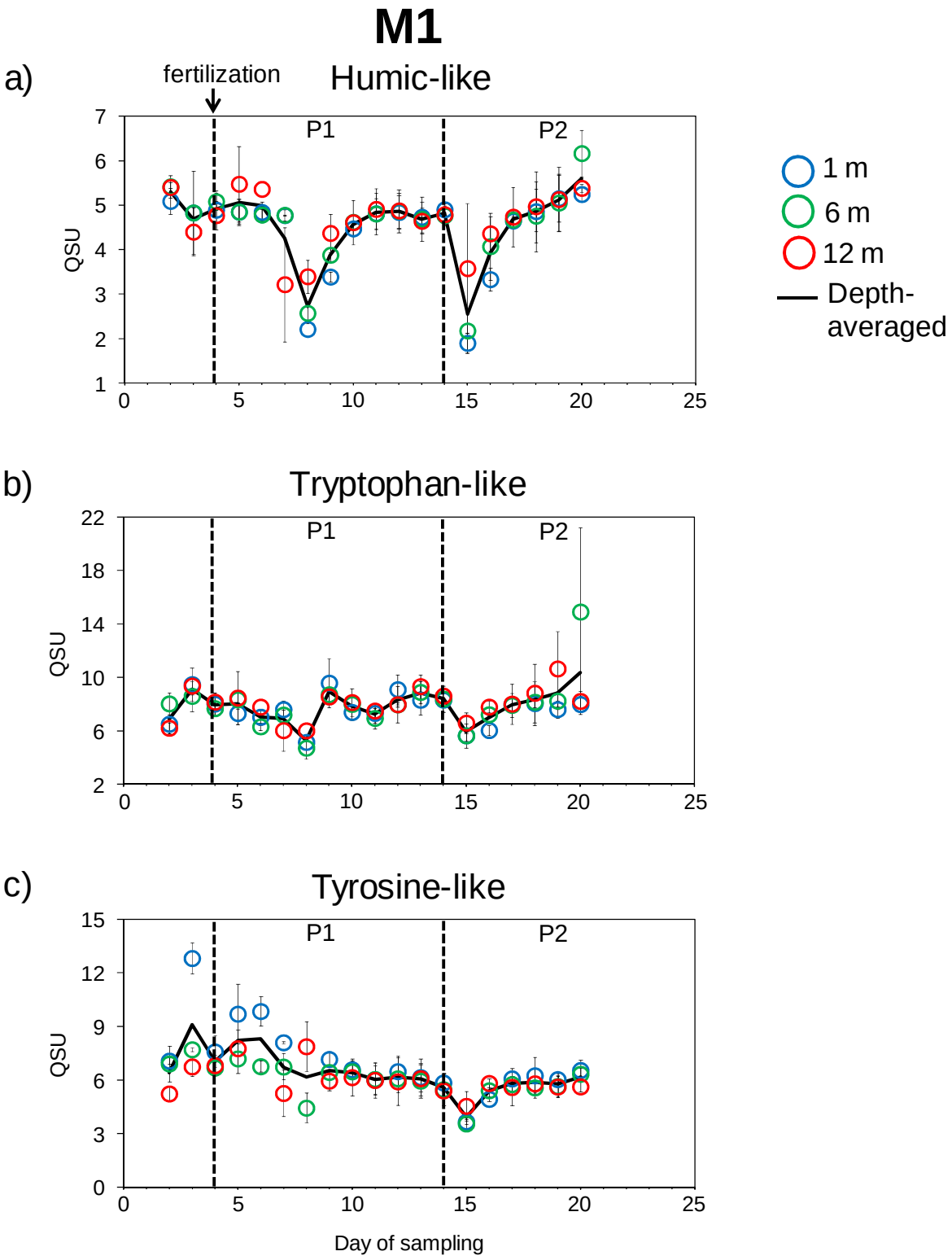
M1
a)
fertilization
Humic-like
P1
P2
QSU
1 m
6 m
12 m
Depth-averaged
b)
Tryptophan-like
c)
Tyrosine-like
Day of sampling

Figure 8

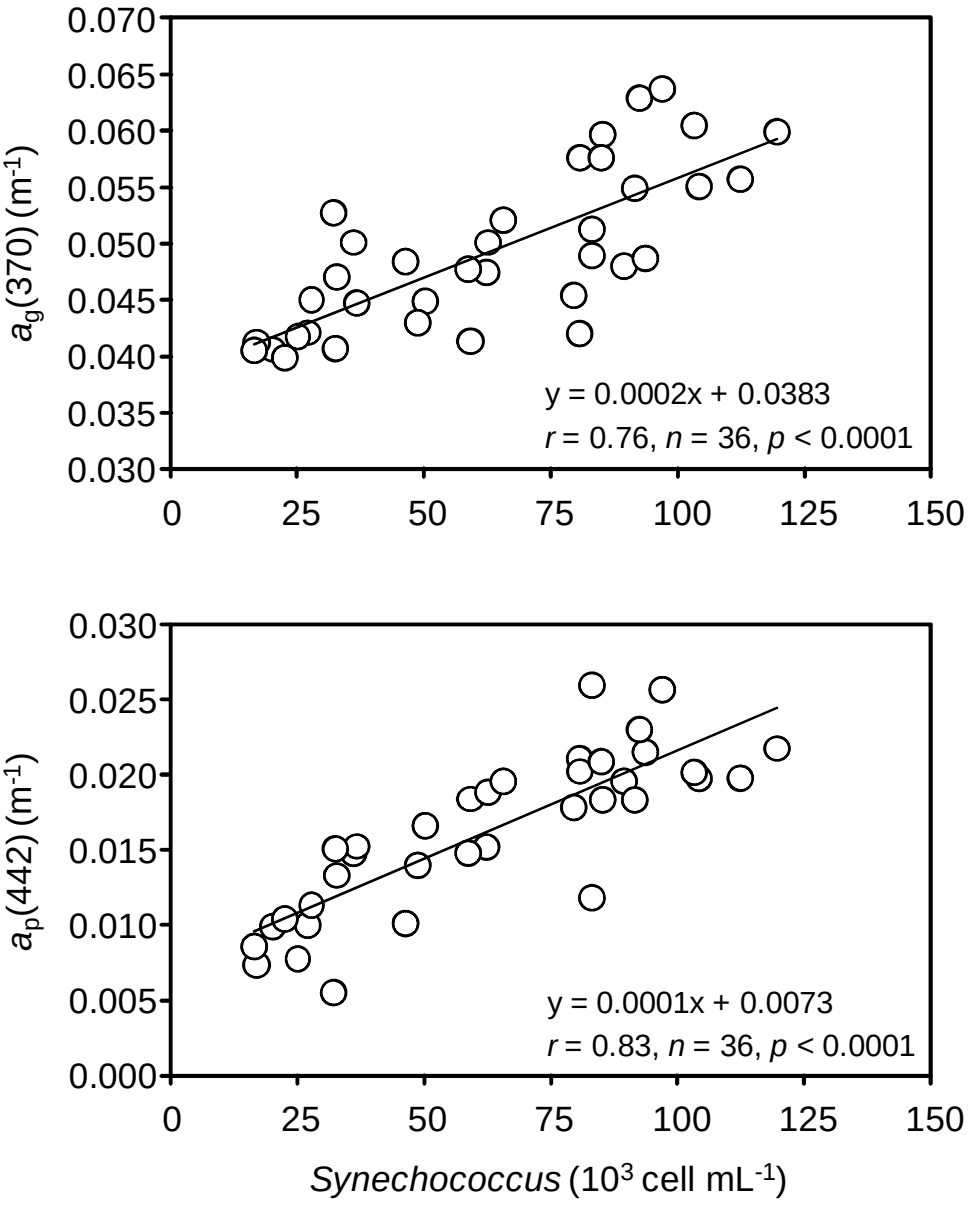
0.070
0.065
0.060
0.055
0.050
0.045
0.040
0.035
0.030
$a_g(370)$ (m^{-1})
y = 0.0002x + 0.0383
r = 0.76, n = 36, p < 0.0001
0
25
50
75
100
125
150
0.030
0.025
0.020
0.015
0.010
0.005
0.000
$a_p(442)$ (m^{-1})
y = 0.0001x + 0.0073
r = 0.83, n = 36, p < 0.0001
0
25
50
75
100
125
150
Synechococcus (10^3 cell mL^{-1})

Figure 9